Running Title: Role of FERONIA in Root Hair Tip-Growth

Functional Characterization of *fer-ts,* a Temperature-Sensitive FERONIA Mutant Allele That Alters Root Hair Growth

Daewon Kim[1, 3], Jiyuan Yang[3], Fangwei Gu[3], Sung Jin Park[3], Jonathon Combs[3], Alexander Adams[2], Heather B. Mayes[2], Jeong Dong Bahk[1] and Erik Nielsen[3]

[1]*Division of Applied Life Sciences (BK21plus), Graduate School of Gyeongsang National University, Jinju 660-701, Republic of Korea*

[2]*Department of Chemical Engineering, University of Michigan, Ann Arbor, MI 48109, USA.*

[3]*Department of Molecular, Cellular, and Developmental Biology, University of Michigan, Ann Arbor, Michigan 48109*

Corresponding author: E. Nielsen; e-mail: nielsene@umich.edu

E.N. conceived the original screening and research plans; J-D.B. and E.N. supervised the experiments; D.K., F.G., S-J.P., and J.C. performed the in planta experiments and microscopy, and A.A. performed structural modeling and was supervised by H.B.M. D.K. wrote the article with contributions of all the authors; E.N. supervised and completed the writing, and agrees to serve as the author responsible for contact and ensures communication.

ABSTRACT

In plants, root hairs undergo a highly-polarized form of cell expansion called tip-growth, in which cell wall deposition is restricted to the root hair apex. In order to identify essential cellular components that might have been missed in earlier genetic screens we identified conditional temperature sensitive (ts) root hair mutants by EMS mutagenesis. Here we describe one of these mutants, *fer-ts* (*feronia-temperature sensitive)*. Mutant *fer-ts* seedlings grew normally at normal temperatures (20˚C), but failed to form root hairs at elevated temperatures (30˚C). Map based-cloning and whole genome sequencing revealed that *fer-ts* resulted from a G41S substitution in the extracellular domain of *FERONIA* (*FER*). A functional fluorescent fusion of FER containing the *fer-ts* mutation localized to plasma membranes, but was subject to enhanced protein turnover at elevated temperatures. While tip-growth was rapidly inhibited by addition of RALF1 peptides in both wild-type and *fer-ts* mutants at normal temperatures, root elongation of *fer-ts* seedlings was resistant to added RALF1 peptide at elevated temperatures. Additionally, at elevated temperatures *fer-ts* seedlings displayed altered ROS accumulation upon auxin treatment and phenocopied constitutive *fer* mutant responses to a variety of plant hormone treatments. Molecular modeling and sequence comparison with other CrRLK1L receptor family members revealed that the mutated glycine in *fer-ts* is highly conserved, but is not located in the recently characterized RALF23 and LORELI-LIKE-GLYCOPROTEIN (LLG2) binding domains, perhaps suggesting that *fer-ts* phenotypes may not be directly due to loss of binding to RALF1 peptides.

Key words: FERONIA, root hair, tip growth, CrRLK1L receptor kinase, RALF.

49 # INTRODUCTION

50 In higher plants, root hairs are cellular protuberances resulting from the polarized
51 outgrowth of specialized root epidermal cells, known as trichoblasts (Gilroy and Jones,
52 2000). Root hair development can be divided into three phases: cell specification,
53 initiation of bulge formation, and polarized tip growth (Cho and Cosgrove, 2002).
54 Polarized tip growth results from highly localized exocytosis of Golgi-derived vesicles
55 containing newly synthesized cell wall material at a restricted area of the root hair tip,
56 with a tip-focused cytoplasmic calcium ion (Ca^{2+}) gradient ensuring correct targeting of
57 this polarized membrane trafficking (Hepler et al., 2001; Smith et al., 2005; Cole and
58 Fowler, 2006). This Ca^{2+} gradient is established by localized generation of reactive
59 oxygen species (ROS) by *ROOT HAIR DEFECTIVE2* (*RHD2*) which encodes an
60 NADPH oxidase in *A. thaliana* (Foreman et al., 2003). RHO OF PLANTS (ROP) small
61 GTPases mediated signal transduction is involved in specifying the root hair initiation
62 site, and future root hair elongation by stimulating *RHD2* activity at the growing root hair
63 apex (Molendijk et al., 2001; Jones et al., 2002; Carol and Dolan, 2006). Recently, a
64 number of receptor-like kinases (RLKs) have been identified that are involved in cellular
65 growth regulatory mechanisms, especially in cell elongation associated with root hair tip
66 growth in higher plants (Shiu and Bleecker, 2001; Lehti-Shiu et al., 2009; Lindner et al.,
67 2012). In particular, CrRLK1L subfamily proteins, which includes *FER* (Huck et al.,
68 2003), *ERELUS* (*ERE*) (Haruta et al., 2014; Schoenaers et al., 2018), *THESEUS1* (*THE1*)
69 (Hematy et al., 2007), *ANXUR1/2* (Miyazaki et al., 2009), have been implicated in cell
70 wall sensing associated with a variety of cellular events such as female fertility, cell
71 elongation, root-hair development, mechanosensing, and responses to hormones and

72 pathogens (Boisson-Dernier et al., 2009; Cheung and Wu, 2011; Lindner et al., 2012).

73 The CrRLK1L subfamily is named after the first member functionally
74 characterized in *Catharanthus roseus* cell cultures (Schulze-Muth et al., 1996), and
75 Arabidopsis, contains 17 CrRLK1L subfamily members (Hematy and Hofte, 2008). The
76 majority of CrRLK1L receptor-like kinase proteins are predicted serine/threonine kinases
77 with a single transmembrane between an N-terminal extracellular domain with two
78 tandem domains showing limited homology to the carbohydrate-binding domain of
79 animal malectin proteins and a C-terminal cytoplasmic kinase domain (Schallus et al.,
80 2008); (Cheung and Wu, 2011). *THE1* was discovered in a screen for suppressors that
81 partially restored the dark-grown hypocotyl growth defect of *procuste1-1(prc1-1)*, which
82 is defective in the cellulose synthase catalytic subunit CESA6 (Hematy et al., 2007), and,
83 *HERCULES1* (*HERK1*), was identified as functionally redundant with *THE1* in
84 modulating cell elongation (Guo et al., 2009). While single mutant *the1* or *herk1* plants
85 displayed normal growth, *the1 herk1* double mutants were severely stunted (Guo et al.,
86 2009). *ANXUR1* and *ANXUR2* (*ANX1* and *ANX2*), are exclusively expressed in the male
87 gametophyte (Boisson-Dernier et al., 2009), and function in maintaining pollen tube wall
88 integrity during migration through floral tissues until their deactivation allows the pollen
89 to burst during fertilization (Boisson-Dernier et al., 2009).

90 Similar to *ANX1* and *ANX2*, *FER*, which is allelic to *SIRÈNE (SRN),* was initially
91 identified in the regulation of female control of fertility (Huck et al., 2003), and is highly
92 expressed in the synergid cells of the female gametophyte and in a variety of vegetative
93 tissues, but not in the male gametophyte (Escobar-Restrepo et al., 2007; Guo et al.,
94 2009). In the female gametophyte, *FER* is involved in sensing pollen tube arrival and
95 promoting its rupture, (Huck et al., 2003; Rotman et al., 2003), and in the initiation of

96 programmed cell death of one of two synergid cells during the double fertilization event
97 (Ngo et al., 2014). *FER* also inhibits polyspermy through regulation of demethylesterified
98 pectin accumulation in the filiform apparatus of the ovule (Duan et al., 2020).

99 In addition to important roles during fertilization, *FER* has also been shown to
100 regulate aspects of root hair elongation (Duan et al., 2010; Huang et al., 2013), calcium
101 signaling during mechanical stimulation of roots (Shih et al., 2014), and cell wall
102 responses to both abiotic and biotic stress (Huck et al., 2003; Rotman et al., 2003; Lindner
103 et al., 2012; Duan et al., 2014; Ngo et al., 2014; Shih et al., 2014; Li et al., 2016). *FER*
104 was identified as a ROP guanidine exchange factor 1 (ROPGEF1) that activates ROP
105 GTPase signaling during root hair tip-growth in Arabidopsis (Duan et al., 2010). *FER*,
106 and other members of the CrRLK1L receptor families have been proposed to bind to
107 secreted RALF (rapid alkalinization factor) peptide ligands (Haruta et al., 2014), with
108 RALF1 binding the *FER* extracellular domain to suppress cell elongation of the primary
109 root (Haruta et al., 2014). RALF34 binds to *THE1* during regulation of lateral root
110 initiation (Gonneau et al., 2018), and RALF23 binding to *FER* negatively regulates plant
111 immune responses (Stegmann et al., 2017). More recently, *FER* was shown to associate
112 with a GPI-anchored co-receptor, *LORELEI* (*LRE*; Liu et al., 2016), and a crystal structure
113 of the FER extracellular domain bound to a LRE-like protein (LLG2), and RALF23
114 shows that LLG2 and RALF23 peptides associate with the second malectin-like domain
115 (Xiao et al., 2019).

116 Although RALF peptide binding occurs in several CrRLK1L receptor-like
117 kinases, it remains unclear whether this is the only ligand recognized by this class of
118 receptor-like kinases. Indeed, *the1-1* mutants displayed altered growth phenotypes
119 despite the *the1-1* mutant extracellular domain being able to bind RALF34 (Gonneau et

120 al., 2018). Additionally, while RALF peptides appear to only bind the second of two
121 malectin-like domains in the FER extracellular domain, both these domains appear to
122 associate with pectin polysaccharides (Feng et al., 2018). We have identified a new
123 temperature-sensitive mutation (*fer-ts*) in a highly conserved glycine residue (G41S)
124 present in the extracellular domain of the FER receptor kinase, as well as other members
125 of the CrRLK1L receptor-like kinase family and mammalian malectin sequences. The *fer-*
126 *ts* mutant exhibited rapid cessation of root hair tip-growth within one minute upon
127 transferal to elevated (30ºC) growth temperatures. This rapid cessation of root hair tip
128 growth was also observed when *fer-4* null mutants were transformed with a fluorescently-
129 tagged version of the temperature-sensitive FER(G41S)-EYFP. FER(G41S)-EYFP was
130 still present in the plasma membrane in root hairs that had ceased tip-growth, indicating
131 that the primary defect of this mutant is due to failure to properly transmit extracellular
132 signals at elevated temperatures. These findings provide a powerful new tool for
133 dissecting how FERONIA, and potentially other CrRLK1L receptor-like kinases,
134 function during plant growth and development.
135

136 # RESULTS

137 **Isolation of a temperature-sensitive mutant that inhibits root hair tip growth**

138 The regulatory GTPase, RabA4b, participates in membrane trafficking associated with
139 the polarized secretion of cell wall components in plant cells. In addition, loss of tip
140 localization of EYFP-RabA4b is highly correlated with inhibition of root hair tip growth
141 (Preuss et al., 2004). In order to identify molecular components that control root hair tip
142 growth, EMS-mutagenized seeds of a stable transgenic Arabidopsis line expressing

143 EYFP-RabA4b were screened for seedlings with wild-type root hairs at normal
144 temperatures (20˚C), but which displayed impaired root hair growth when grown at
145 elevated temperatures (30˚C). The progeny of approximately 6,000 EMS-mutagenized
146 seeds were screened. From the screening, four temperature-sensitive (ts-) root hair growth
147 defect mutants were isolated, which we initially termed Loss-of-Tip-Localization mutants
148 (*ltl1* to *ltl4*). Among these *ltl ts* mutants, *ltl2*, (subsequently referred to as *fer-ts*) root hair
149 growth characteristics were examined under normal and elevated temperature conditions.
150 In normal growth conditions (20˚C), *fer-ts* root hairs displayed normal growth, however,
151 both root hair growth and apical accumulation of EYFP-RabA4b of *fer-ts* root hairs were
152 dramatically inhibited at 30˚C (Figure 1a and 1b).

153 To quantify root hair elongation in *fer-ts* under normal and elevated temperature
154 conditions, both root hair lengths and root hair density were measured. No significant
155 differences were found between wild-type and *fer-ts* either in mature root hair length, or
156 in the number of root hairs per unit root length when plants were grown at 20˚C. However,
157 both length of root hairs and root hair density were greatly reduced in *fer-ts* in plants
158 grown at 30˚C (Figure 1c and 1d). Primary root length and root growth rates of *fer-ts*
159 seedlings were indistinguishable from wild-type at 20ºC, but while wild-type roots grew
160 slightly faster at 30ºC, *fer-ts* primary root growth rates remained unchanged at elevated
161 temperatures (See Supplemental Figure S1). These results indicated that, at least in early
162 stages of seedling growth and development *fer-ts* temperature sensitive defects are largely
163 specific to root hair elongation in elevated temperature conditions.

164 In order to characterize effects of the *fer-ts* mutation on root hair growth
165 dynamics, elongating root hairs were visualized by time-lapse microscopy for two hours.
166 Seven day-old *fer-ts* seedlings were placed in a temperature-controlled plant growth

167 chamber at 20˚C for 50 min and then the temperature of the chamber was rapidly
168 transitioned to 30˚C (Figure 2). While root hair growth was unaffected by temperature
169 transition in wild-type plants, transition from normal to elevated temperatures resulted in
170 rapid cessation of tip-growth in the *fer-ts* mutant (Figure 2 and Movie S1).

171 Since root hair growth is tightly linked to accumulation of EYFP-RabA4b
172 compartments in root hair tips (Preuss et al., 2004; Preuss et al., 2006; Thole et al., 2008),
173 we were interested how this localization was affected upon transition from 20ºC to 30ºC
174 in the *fer-ts* mutants. EYFP-RabA4b was detected in the apical region of growing *fer-ts*
175 root hairs at 20˚C, but tip localization of EYFP-RabA4b was rapidly lost upon transition
176 to 30˚C (Figure 3). EYFP-RabA4b accumulation was examined in wild-type and *fer-ts*
177 plants in a temperature-controlled chamber at 20˚C for 14 min, and then the chamber was
178 rapidly transitioned to 30˚C (Figure 3a and Supplemental Figure S2). Images of growing
179 root hairs were collected at one minute intervals by time-lapse confocal microscopy, and
180 tip-localized EYFP signal was quantified in both wild-type (Figure 3b) and *fer-ts* (Figure
181 3c) root hairs. While tip-localized EYFP-RabA4b signal was unaffected by transition
182 from 20˚C to 30˚C in wild-type root hairs (Figure 3b), tip-localized EYFP-RabA4b was
183 significantly reduced in *fer-ts* within one minute of the transition from 20˚C to 30˚C
184 (Figure 3c).

185

186 **Map-based cloning and full-genome sequencing of the *fer-ts* locus**

187 To identify the mutant locus responsible for the rapid, temperature-sensitive loss of root
188 hair elongation and tip-localized EYFP-RabA4b, map-based cloning and full-genome
189 sequencing was performed. F_2 mapping populations were obtained by reciprocal crosses
190 of back-crossed mutants (Col-0) with L*er* wild-type plants (Bell and Ecker, 1994).

191 Segregating F_2 populations were used for the subsequent map-based cloning. The
192 temperature-sensitive mutant lesion was mapped to chromosome 3 between the SSLP
193 markers *NIT1.2* and *NGA6* (Figure 4a). Subsequent low-resolution mapping and whole
194 genome sequencing identified that the *fer-ts* mutant locus was due to a G121A nucleotide
195 replacement resulting in a G41S substitution mutation within the extracellular domain of
196 the previously characterized FER receptor-like kinase (Figure 4b and 4c). In order to
197 eliminate the possibility that the G→A substitution that gave rise to the *fer-ts* G41S
198 mutation influenced accumulation of *FER* mRNA at the transcriptional level, we
199 performed RT-PCR analysis. *FERONIA* transcript levels were unchanged from those in
200 wild-type plants (Figure 4d).
201

202 **The G41S mutation in *fer-ts* is a highly conserved glycine residue in CrRLK1L**
203 **subfamily proteins**

204 The G41S substitution of the *fer-ts* mutant rapidly inactivated *FER* function during root
205 hair growth at elevated temperatures. In addition, a similar G37D mutation is responsible
206 for inactivation of THE1, another member of the CrRLK1L family (Hematy et al., 2007),
207 and multiple sequence alignment analysis with other Arabidopsis CrRLK1L family
208 members and animal malectin sequences showed that the G41 residue of FERONIA is
209 absolutely conserved in these malectins and malectin-like 1 (ML1) domains (Figure 5a,
210 and Supplemental Figure S3). Interestingly, based on structural studies of animal malectin
211 proteins, five key residues (Y67, Y89, Y116, F117, D186; Figure 10b, red residues) were
212 found to form contacts with a bound disaccharide ligand, nigerose, in the active site as
213 determined by structural analysis of the *X. laevis* malectin protein (Schallus et al., 2008;
214 Muller et al., 2010). In this malectin structure these surface exposed residues extend from

215 the malectin fold forming the nigerose binding pocket, with the conserved glycine (G40)
216 the bottom of this structural region (Figure 5b). While several of the tyrosine and
217 phenylalanine residues shown to be important for interaction with carbohydrates in
218 animal malectin proteins are maintained in plant malectin-like domains (e.g. FERONIA
219 Y88, Y114, F115, D197) (Figure 5a, and Supplemental Figure S3), these are not surface
220 exposed in the ML1 domain of the recently described crystal structure of FER (Figure 5c,
221 in green) with its co-receptor LLG2 (Figure 5b, in blue) and a RALF23 ligand (Figure 5c,
222 in magenta) (Xiao et al., 2019). It is however notable that in this structure the invariant
223 glycine (G41; Figure 5c, red residue) of the FER ML1 domain is not located within or
224 nearby the RALF23 and LLG2 binding surfaces in the ML2 domain (Xiao et al., 2019).
225

226 ***fer-ts* phenotypes were confirmed by reciprocal crossing with FERONIA mutants**
227 **and complementation assays**

228 To confirm that the temperature sensitive root hair defects and loss of tip-localized EYFP-
229 RabA4b were causally linked to the G41S mutation in the FER locus, *fer-ts* mutant plants
230 were reciprocally crossed with two previously characterized *FER* mutants, *fer-4* and *fer-*
231 *5* (Duan et al., 2010). While both *fer-4* and *fer-5* fail to accumulate root hairs, *fer-4* was
232 shown to fully abolish FER protein, while *fer-5* was shown to accumulate a truncated
233 FER protein missing a functional cytosolic protein kinase domain (Duan et al., 2010). As
234 a control, F1 plants of *fer-ts* crossed to wild-type plants displayed normal root hair growth
235 in both normal and elevated temperature conditions, confirming that the *fer-ts* mutation
236 is recessive. However, F1 plants of either *fer-ts* (paternal line) crossed with *fer-4* and *fer-*
237 *5* mutants (maternal lines; Figure 6a), or *fer-ts* (maternal line) crossed with *fer-4* and *fer-*
238 *5* mutants (paternal line; Supplemental Figure S4a) displayed ts-phenotypes at elevated

239 temperatures, respectively. These F1 plants were confirmed by genomic DNA PCR
240 analysis with primers that discriminated between the *fer-ts* (or wild-type) *FER* loci and
241 *fer-4* and *fer-5* T-DNA insertion mutant loci (Figure 6b-c, and Supplemental Figure S4b).
242 To verify that the FER G41S mutation specifically conferred the temperature-sensitive
243 root hair phenotype, a fluorescently tagged FER-EYFP containing the G41S mutation,
244 FER(G41S), driven by endogenous *FER* promoter sequences, was transformed into *fer-4*
245 and *fer-5* mutant plants. Transgenic *fer-4* and *fer-5* plants, expressing mutant
246 FER(G41S)-EYFP proteins rescued root hair growth defects in these two *fer* mutant
247 backgrounds in a temperature-sensitive manner (Figure 6d). Finally, a wild-type
248 fluorescently-tagged FER-EYFP, driven by endogenous FER promoter sequences, was
249 able to fully rescue *fer-ts* root hair defects. FER(WT)-EYFP protein was detected in
250 plasma membranes and *fer-ts* transgenic lines stably transformed and homozygous for
251 FER(WT)-EYFP displayed the normal root hair growth both 20˚C and 30˚C (Figure 6e).
252 As observed previously (Duan et al., 2010), pFER-FER(WT)-EYFP fluorescent fusions
253 localized primarily to plasma membranes in both root cortical and mature root hair cells
254 in these transgenic lines, although a small amount of pFER-FER(WT)-EYFP could also
255 be seen in subcellular compartments that colocalized with FM 4-64 (Figure 6f) Taken
256 together, these data strongly support that *fer-ts* phenotype is the result of the G41S
257 mutation of the FERONIA protein.
258

259 **FERONIA is primarily localized to the plasma membranes and the *fer-ts* G41S**
260 **substitution does not alter its subcellular localization**

261 Previously, GFP-fused FERONIA was shown to localize to plasma membranes in various
262 plant tissues (Duan et al., 2010). At normal temperatures, FER(WT)-EYFP was observed

263 primarily in plasma membranes in various tissues such as leaf, root and in mature root
264 hairs (Figure 6f and 7a), and at higher magnification in root cortical cells FER(WT)-
265 EYFP was restricted to plasma membranes, and did not display significant accumulation
266 in intracellular compartments in non-tip-growing root cortical cells (Figure 7b).
267 Interestingly, in actively growing root hairs, FER(WT)-EYFP protein was observed both
268 in plasma membranes and an apical localized vesicle population in growing root hairs
269 (Movie S2). To determine whether the introduction of the G41S substitution in the *fer-*
270 *ts* mutant might affect the subcellular localization of this protein in normal or elevated
271 temperatures, we compared the subcellular distributions of FER(WT)-EYFP and
272 FER(G41S)-EYFP at both 20˚C and 30˚C (Figure 7c and 7d). While no changes in
273 accumulation or distribution of FER(WT)-EYFP were observed in roots and mature root
274 hairs between 20ºC and 30ºC conditions (Figure 7c), at 30ºC some FER(G41S)-EYFP
275 fluorescence could be observed in internal subcellular membranes, although significant
276 levels of the FER(G41S)-EYFP remained at the plasma membranes in these cells even
277 after incubation at 30˚C for 6 hours (Figure 7e).

278 Since the *fer-ts* phenotype rapidly inhibited tip-growth upon transition to elevated
279 temperatures (30ºC), we were interested to determine how this might effect FER(G41S)-
280 EYFP localization in actively growing root hair cells. Seven day-old *fer-ts* seedlings
281 were placed in a temperature-controlled plant growth chamber at 20˚C and images of
282 growing root hairs of plants stably expressing FER(WT)-EYFP or FER(G41S)-EYFP
283 were collected every five seconds for at least five minutes, and then the temperature of
284 the chamber was rapidly transitioned to 30˚C (Figure 8a) to observe the effects of elevated
285 temperatures on both root hair elongation as well as subcellular dynamics of FER(WT)-
286 EYFP and FER(G41S)-EYFP proteins. As noted previously, both EYFP(WT)-EYFP and

287 FER(G41S)-EYFP localized to both plasma membranes and apically-localized vesicle
288 populations in growing root hairs at 20ºC (Figure 8a and Movie S3). However, while
289 root hair growth and FER(WT)-EYFP localization were unaffected by elevated
290 temperature (30ºC), both tip-growth and accumulation of apically-localized vesicles were
291 inhibited within one minute of transition to elevated temperature (Figure 8c, 8d, and
292 Movie S3). While FER(G41S)-EYFP in apically-localized vesicles was rapidly lost upon
293 cessation of tip-growth, plasma membrane localized FER(G41S)-EYFP levels were
294 maintained at similar levels for several minutes at elevated temperatures. Interestingly,
295 after several minutes of elevated temperature the ratio of FER(G41S)-EYFP localized in
296 an apical plasma membrane domain (Figure 8b, red) versus in flanking plasma membrane
297 regions (Figure 8b, blue) declined (Figure 8e), perhaps reflecting either inhibition of
298 secretion to this apical domain, or possibly due to destabilization of the FER(G41S)-
299 EYFP protein at elevated temperatures.

300 In order to examine whether the *fer-ts* mutant protein might display increased
301 protein turnover we blocked new protein synthesis by treating five-day-old *Arabidopsis*
302 seedlings with cycloheximide, and then compared protein turnover rates of the FER(WT)-
303 EYFP and FER(G41S)-EYFP proteins when grown at 30ºC. Overall accumulation of the
304 FER(G41S)-EYFP was reduced significantly during the time course, but no significant
305 reduction in protein accumulation was observed for either EYFP(WT)-EYFP or an actin
306 loading control (Figure 8f). These results suggest that while rapid cessation of tip-growth
307 in root hairs occurs within one minute of transition to elevated temperatures, that upon
308 continuous incubation at elevated temperatures *fer-ts* mutant proteins also appear to be
309 subject to enhanced protein turnover.

310

311 **The *fer-ts* displays impaired sensitivity to RALF1 peptides in elevated temperature**
312 **conditions**

313 Signaling in the CrRLK1L family of receptor kinases have been linked to a family of
314 small extracellular peptide hormones called rapid alkalinization factors (RALFs; (Haruta
315 et al., 2014; Stegmann et al., 2017). RALF1, which was previously demonstrated to
316 suppress cell elongation of the primary root in Arabidopsis and other plants (Pearce et al.,
317 2001), has now been shown to directly bind with the FER extracellular domain (Haruta
318 et al., 2014; Stegmann et al., 2017). Because the G41S mutation in *fer-ts* appears to
319 rapidly inhibit tip-restricted growth at elevated temperatures, perhaps by destabilizing the
320 structure of the extracellular domain of this protein (Figure 8f), we were curious what
321 effect RALF1 peptide might have on root hair growth, and whether the *fer-ts* mutant may
322 display altered responses to RALF1 peptide treatments at elevated temperatures (30ºC).
323 Treatment of growing *fer-ts* and wild-type (Figure 9a and Movie S4) root hairs resulted
324 in rapid cessation of tip-growth (<1 min; Figure 9b) in normal temperatures (20ºC).

325 Because *fer-ts* root hair growth was already inhibited at 30ºC it was not possible
326 to measure RALF1 peptide effects in root hair cells. However, since primary root
327 elongation did not appear to be as dramatically affected at elevated temperatures as root
328 hair growth (30ºC; Figure S1), we examined the temperature-dependent effect of RALF1
329 peptide treatment on these tissues. As shown in Figure 10, both wild-type seedlings and
330 *fer-ts* mutants were highly sensitive to active RALF1 peptide under normal temperature
331 conditions (20ºC). However, as previously described, the sensitivity of root growth to
332 RALF1 in the *fer-5* mutant was reduced in comparison to wild-type plants at 20ºC (Figure
333 10a and 10c). Importantly, sensitivity of *fer-ts* seedlings to RALF1 peptide treatment was
334 dramatically reduced at 30ºC, even though wild-type plants and *fer-5* mutants still

335 responded to RALF1 peptide treatment with similar levels of root elongation inhibition
336 (Figure 10b and 10d). These results support the previous determination that RALF1
337 peptide signaling occurs through the FER receptor-like kinase, and would be consistent
338 with the G41S mutation resulting in temperature-sensitive inhibition of RALF1-mediated
339 FERONIA signaling.
340
341 **ROS accumulation of *fer-ts* was greatly reduced at 30 ºC and *fer-ts* phenotype was**
342 **not rescued by various hormone treatments.**
343 In previous reports, ROS accumulation is highly reduced in *fer-4* and *fer-5* mutants
344 especially in root hair tips and primary roots (Duan et al., 2010). In order to investigate
345 the ROS accumulation, WT and *fer* mutants were treated with H_2DCF-DA to monitor
346 ROS levels. In WT plants, ROS accumulation was observed in primary roots and root
347 hairs, and in root hairs these levels increased slightly upon NAA treatment at both 20ºC
348 and 30ºC (Figure 11). While *fer-ts* plants showed similar ROS accumulation patterns as
349 those observed in wild-type plants at 20ºC, at 30ºC ROS accumulation was dramatically
350 reduced both in the absence and presence of NAA (Figure 11a). However, while ROS
351 accumulation in the *fer-ts* mutant was strictly temperature dependent (compare Figures
352 11b and 11c), these reduced ROS levels were similar to those observed at both
353 temperatures for the constitutive *fer-4* and *fer-5* mutants (Figure 11a; compare Figures
354 11b and 11c)
355 In order to investigate how broadly the temperature-sensitive *fer-ts* mutant
356 phenocopied *fer-4* and *fer-5* mutants, these three mutants were treated with several
357 different concentrations of hormones, and then root hair lengths and densities were
358 measured either at 20ºC or 30ºC. Root hair lengths and densities displayed the similar

359 patterns for both wild-type and *fer-ts* at 20ºC, while both *fer-4* and *fer-5* root hairs were
360 consistently shorter and less dense (Supplemental Figure S5a and S5b; upper panels).
361 However at 30ºC, *fer-ts* root hair lengths and densities largely resembled the *fer-4* and
362 *fer-5* phenotypes (Supplemental Figure S5a and S5b; lower panels). Primary root length,
363 total lateral root number, fresh weight, and total leaf numbers of *fer-ts* mutants also
364 displayed a similar temperature-dependent trend; resembling wild-type plants with
365 various hormone treatments at 20ºC, but resembling *fer-4* and *fer-5* mutants at 30ºC (See
366 supplemental Figure S6).
367
368

369 **DISCUSSION**

370 In eukaryotes, receptor like kinases (RLKs) have been implicated to play an important
371 role in many crucial eukaryotic cellular processes, such as cell cycle progression, cell
372 signaling, embryogenesis, abiotic and biotic stress responses (Shiu and Bleecker, 2001;
373 Morillo and Tax, 2006; Lehti-Shiu et al., 2009). In this study, we isolated and identified a
374 temperature-sensitive root hair elongation mutant, which we have determined is a new
375 mutant *FER* allele that we have called *fer-ts*. The *fer-ts* mutant displays normal overall
376 growth characteristics at normal temperature (20˚C), but root hair initiation and
377 elongation are specifically and rapidly inhibited within one minute upon transfer of these
378 plants to elevated temperature (30˚C). We have shown that the *fer-ts* mutant is the result
379 of a substitution mutation in which a highly conserved glycine residue in the FER
380 extracellular domain is changed to serine (G41S). FERONIA is a member of the
381 CrRLK1L subfamily of receptor-like kinases (RLKs) in *Arabidopsis* and the mutated
382 glycine residue (G41S) is highly conserved in multiple members of the CrRLK1L family

383 of receptor proteins as well as in animal malectin proteins.

384 While both FER(WT)-EYFP and FER(G41S)-EYFP fusion proteins displayed a
385 plasma membrane localization at both normal and elevated temperatures, FER(G41S)-
386 EYFP displayed significantly increased protein turnover 30ºC (Figure 6). However, this
387 increased protein turnover did not appear to result in loss of accumulation of FER(G41S)-
388 EYFP in plasma membranes. This is likely due to continued protein synthesis and at least
389 some secretion of these proteins at the elevated temperature. These results, along with the
390 rapid cessation of root hair elongation (<1 min) in elevated temperatures would be
391 consistent with rapid inactivation of FER signaling activity due to protein inactivation
392 rather than simply depletion of FER activity from the plasma membrane due to increased
393 turnover.

394 *FER* has been implicated in a variety of plant processes, including roles in root
395 hair tip growth as well as crucial plant processes, such as pollen tube reception, hypocotyl
396 elongation, regulation of ABA signaling and controlling seed size (Escobar-Restrepo et
397 al., 2007; Deslauriers and Larsen, 2010; Duan et al., 2010; Yu et al., 2012; Yu et al., 2014).
398 In many of these processes, FER signaling appears to regulate ROS production. In
399 constitutive *fer* mutants, ROS levels are reduced, and FER overexpression results in
400 increased ROS levels. The observation that the *fer-ts* mutant also displays reduced ROS
401 levels only at elevated temperatures suggests that this mutation affects FER signaling in
402 a similar fashion as other *fer* mutants, perhaps providing a powerful tool for elucidation
403 of downstream signaling events associated with FER function, and indicating that at least
404 one important downstream effect of *FER* signal transduction is regulation of ROS
405 production. This was elegantly explained by the discovery that FER recruits ROPGEFs,
406 which in turn activate ROP GTPases, leading to the stimulation of RHD2 NADPH

407 oxidase dependent ROS production (Duan et al., 2010). Therefore, FER mediated
408 regulation of ROS production is likely important and tightly controlled for many cellular
409 functions.

410 Based on sequence comparison, the extracellular domains of members of the
411 CrRLK1L subfamily of plant RLK proteins were predicted to share some structural
412 similarity to the mammalian malectin protein (Schallus et al., 2008). Malectin was first
413 identified and characterized in *X. laevis* as carbohydrate binding protein of the
414 endoplasmic reticulum where it plays an important role in the early steps of protein N-
415 glycosylation for biogenesis of glycoproteins (Schallus et al., 2008). Based on NMR
416 structure analysis, there are five key residues in the malectin domain (Y67, Y89, Y116,
417 F117, D186) that are located in pocket-shaped structure and these aromatic residues and
418 the aspartate mediate interactions with the glucose residues of maltose and nigerose di-
419 saccharide ligands (Schallus et al., 2008). In plants, malectin-like domains are mainly
420 found in CrRLK1L subfamily with a low overall sequence identity with animal malectins
421 (Shiu and Bleecker, 2003). In FER, two malectin-like domains, ML1 and ML2, are
422 found as a tandem-repeat in the extracellular domain. Interestingly, several key residues
423 found in the ligand-binding pocket of the animal malectin structure are maintained in the
424 malectin-like domains of FER and other plant CrRLK1L family members (Schallus et al.,
425 2008). However, the discovery that members of a family of small secreted peptides,
426 RALFs, rather than cell wall polysaccharides or oligosaccharides, serve as important
427 ligands for FER and other CrRLK1L family receptors (Haruta et al., 2014; Ge et al., 2017;
428 Stegmann et al., 2017; Gonneau et al., 2018) might indicate that these extracellular
429 domains may interact with ligands in a manner distinct from their animal counterparts.
430 Indeed the recent structural characterization of ANX1/2 extracellular domains (Du et al.,

431 2018) and the FER extracellular domain in complex with RALF23 and the FER co-
432 receptor, LLG2 (Xiao et al., 2019) has shown that the RALF23 binding domain and
433 interaction with LLG2 occurs primarily with the ML2 domain, and that conserved
434 tyrosine and phenylalanine residues in CrRLK1L malectin folds in these structures appear
435 to be buried within the ML1 fold, and therefore likely unavailable to interact with cell
436 wall carbohydrates in a manner similar to animal malectins.

437 On the other hand, analysis of the animal and plant malectin domains, reveals an
438 additional invariant glycine residue, that is present in all animal and plant malectin
439 sequences, and which is also found in close proximity to pocket-shape ligand-binding
440 cleft determined in the structure of the animal ML1 domain. This invariant glycine is
441 replaced with a serine (G41S) in the *fer-ts* mutation described in this paper. The highly
442 conserved nature of this glycine residue, and the rapid elimination of FER signaling at
443 elevated temperatures, suggests a critical role for the FER ML1 domain in ligand binding
444 or transduction of a ligand-binding signal in members of the CrRLK1L family of receptor-
445 like kinases. Indeed, mutation of an analogous glycine residue to aspartic acid (G37D) in
446 the extracellular domain of THESEUS in the *the1-1* mutant also results in a loss of
447 function mutation in this RLK (Hematy et al., 2007). The *the1-1* mutation also results in
448 its insensitivity to its specific RALF ligand, RALF34 (Gonneau et al., 2018). However,
449 RALF34 was still found to bind the extracellular domain of *the1-1* containing the G37D
450 mutation in vitro, suggesting that mutation of this glycine residue did not directly impact
451 RALF34 binding (Gonneau et al., 2018). Similarly, the response of *fer-ts* mutant to
452 treatment with RALF1 peptide was dramatically reduced under elevated temperature
453 conditions (Figure 7). Precisely how the G41S *fer-ts* mutation, which is not found within
454 the RALF23 peptide binding surface in the FER ML2 domain, would directly block

455 RALF peptide perception and signaling is unclear. One potential explanation may involve
456 the recent discovery of links between *FER* signaling and pectin dynamics during salt
457 stress (Chen et al., 2016; Feng et al., 2018) and fertilization events (Duan et al., 2020).
458 During salt stress, *FER* appears to sense cell wall softening and both FER ML1 and FER
459 ML2 domains were shown to directly interact with pectin *in vitro* (Feng et al., 2018).
460 More recently, *FER* function was shown to be required in order to maintain de-esterified
461 pectin levels in the filiform apparatus during pollination and fertilization events (Duan et
462 al., 2020), Whether the G41S mutation in *fer-ts*, or other analogous mutations of this
463 invariant glycine residue in other CrRLK1L receptors affect the ability of these receptors
464 to interact with or regulate pectin dynamics in plant cell walls is an intriguing possibility
465 that warrants future investigation.
466

467 # EXPERIMENTAL PROCEDURES

468 **Plant materials and growth conditions**

469 *Arabidopsis thaliana* ecotype Columbia (Col-0), the *fer-ts* mutant was isolated from an
470 EMS mutagenized population of wild-type (Col-0) stably transformed with a single copy
471 of EYFP-RabAb4 driven by a 35S promoter (Preuss et al., 2004; Weigel and Glazebrook,
472 2006), and two FERONIA T-DNA insertional mutants (designated as *fer-ts* and two T-
473 DNA insertion mutants, *GABI-GK106A06* (designated as *fer-4*) and *SALK_029056c*
474 (designated as *fer-5*) (Duan et al., 2010) were used in this study. Seeds were sterilized by
475 soaking in 1% bleach solution for 10 min; after washing five times with sterilized water,
476 they were sown onto agar plates for germination. Five- to seven-day-old *A. thaliana*
477 seedlings used in the root-hair growth assays were grown vertically on plates containing

478 0.25x Murashige and Skoog (MS; Sigma-Aldrich) medium at pH 5.7 supplemented with
479 0.6% (w/v) phytagel at 20˚C under long day conditions (16-h days with 150 $\mu E \cdot m^{-2} \cdot s^{-1}$ (E,
480 Einstein; 1 E = 1 mol of photons). For harvesting seeds, seedling plants were transferred
481 to soil and grown to maturity at 20ºC under long day conditions.
482

483 **Quantification of root hair elongation in *fer-ts* under normal and elevated**
484 **temperatures**

485 To characterize root hair growth defective phenotypes in the *fer-ts* mutant, bright-field
486 microscopy was carried out using a Nikon Eclipse E600 wide-field microscope with a
487 10x Plan Apo (0.45 NA) lens as previously described in (Preuss et al., 2004). The *fer-ts*
488 mutants were germinated and grown vertically on plates containing 0.25x MS medium at
489 pH 5.7 supplemented with 0.6% (w/v) phytagel at 20ºC for 7 days and then transferred to
490 30ºC and grown for 6 hours before returning back to 20ºC growth conditions for an
491 additional 24 hours, when images of roots and root hairs were then collected. Time-lapse
492 video microscopic analysis was carried out under normal and elevated temperature
493 conditions in wild-type and *fer-ts* mutants as described previously (Preuss et al., 2004).
494 Images of growing root hairs were collected from seedlings by time-lapse video
495 microscopy either using a Nikon Eclipse E600 wide-field microscope with a 10x Plan
496 Apo (0.45 NA) lens (for bright-field images), or using a Leica confocal laser-scanning
497 microscope SP8 with a 63x oil lens (1.4 NA). YFP fluorescence was excited at 514 nm
498 and visualized from 519 nm to 650 nm (Yang et al., 2020). The temperatures of MS
499 medium was controlled by an inline single-channel automatic temperature controller
500 (Werner Instruments, Hamden, CT, model:TC-324B) controlled by a dry air thermostat
501 inserted into the growth chamber and situated approximately 2 mm from the ROI.

502 Temperatures were actively recorded using an Infrared Thermometer (Kintrex Inc.,
503 Vienna, VA, model:IRT0424). Raw image sequences were cropped with Adobe
504 Photoshop and imported into Fiji-ImageJ (Schindelin et al., 2012) to generate time
505 projections using the Stacks function. Quantification of root-hair lengths, growth rates,
506 and densities were quantified by using calibrate and measure functions.
507

508 **Map-based cloning and full genome sequencing of *fer-ts***

509 Self-fertilized, backcrossed *fer-ts* (ecotype; Columbia) mutants were crossed with
510 Landsberg wild-type plants to generate a mapping population. F_1 crossed plants were
511 checked for heterozygosity with the SSLP marker "nga8" that is polymorphic between
512 Col-0 and L*er* (Bell and Ecker, 1994). Homozygous *fer-ts* plants were selected from the
513 segregating F2 population by germination on MS media plates at 20ºC, and subsequent
514 analysis of root hair tip growth defective phenotypes in elevated growth temperatures
515 (30ºC). Homozygous plants displaying *fer-ts* phenotypes were grown to maturity at 20ºC
516 and seed were collected. Genomic DNA was isolated using Qiagen Plant DNA mini kits,
517 and SSLP markers were used for rough mapping the *fer-ts* mutant lesion, which was
518 initially located on chromosome 3 between the SSLP markers *NIT 1.2* and *NGA6*. Low-
519 resolution mapping narrowed the location of the *fer-ts* mutant locus to an approximately
520 2 Mb region of chromosome 3, and full genome sequencing was performed to further
521 determine the *fer-ts* mutation within this region. Libraries were generated for both the *fer-*
522 *ts* and wild-type (ecotype Columbia) extracted DNA using Illumina TruSeq DNA kits
523 and barcoded for multiplexing by the University of Michigan DNA Sequencing Core.
524 Samples were sequenced on an Illumina MiSeq platform with paired-end 150 bp cycles.
525 Sequence reads were checked for quality using FastQC then aligned to the TAIR9 genome

526 using Bowtie2. Potential SNPs were identified using Freebayes. Additional analysis of
527 sequence variants within the low-resolution mapped 2 Mb region of chromosome 3 to
528 eliminate SNPs common to our re-sequenced Col-0 population and the *fer-ts* allele were
529 sorted for context and predicted effect using a custom PERL script.
530

531 **Fluorescence microscopic analysis**

532 For pFER-FER(WT)-EYFP and pFER-FER(G41S)-EYFP transgenic plants, full-length
533 of *FERONIA* including approximately 2 kb promoter was prepared by PCR reaction and
534 sub cloned into the pCAMBIA-EYFP-C1 expression vector (Preuss et al., 2004). Wild-
535 type and mutant FERONIA sequences were amplified from genomic DNA isolated from
536 wild-type and *fer-ts* mutant plants using PCR. To produce pFER-FER(WT)-EYFP and
537 pFER-FER(G41S)-EYFP transgenic plants, these constructs were introduced into *A.*
538 *tumefaciens* strain GV3101, and *Arabidopsis* plants were transformed with *A.*
539 *tumefaciens* using the 'floral-dip' method (Clough and Bent, 1998). Transgenic plants for
540 each construct were selected by germination on 25 mg/L of hygromycin-containing
541 medium (Duchefa, Haarlem, The Netherlands) under long day conditions (16 h light/8 h
542 dark cycle) at 20˚C. Three or more independent, homozygous transgenic lines were
543 isolated for each of the pFER-FER(WT)-EYFP and pFER-FER(G41S)-EYFP constructs
544 in the *fer-ts*, *fer-4*, and *fer-5* mutant backgrounds, respectively, and a single representative
545 homozygous line was used in these studies. Confocal images were generated using a laser
546 confocal microscope (Zeiss Observer.A1) connected to a CSU10 confocal scanner unit
547 (Yokogawa, Japan) and a 10x Plan-Neofluar (0.3 NA lens), 40x Plan-Apochromat (1.3
548 NA lens) or 100x Plan-Apochromat (1.46 NA lens) oil objective with 491 nm laser
549 excitation and a 535 nm emission filter for EGFP and EYFP fluorescence. To visualize

550 cell walls seedlings were incubated for five minutes in Propidium Iodide (10 μg/ml) and
551 then washed with 0.25xMS media, cell membranes were stained with FM 4-64 (5 μM)
552 for five minutes before washing with 0.25xMS media. Images were collected with a
553 Hamamatsu C9100-50 camera operated using the Volocity software version 5 (the
554 electron-multiplying (EM)-CCD detector gain settings were 123, 116 and 190 for images
555 collected with 10x, 40x and 100x objectives, respectively).
556
557 **RT-PCR analysis**
558 For detection of *FERONIA* expression in wild-type, *fer-4*, *fer-5* and *fer-ts* plants, plants
559 frozen immediately in liquid nitrogen. Two microgram aliquots of total RNA extracted
560 from the wild-type or mutant seedlings were used for reverse transcription primed by
561 oligo(dT). Superscript III (Invitrogen, USA) was used for the reverse transcription
562 reaction according to the manufacturer's instructions. One microliter aliquot of the
563 reaction mixture was used for subsequent PCR analysis. *Actin* was used as a quantifying
564 control.
565
566 **Detection of ROS in roots**
567 ROS detection by using H_2DCF-DA in root hair and primary root was performed
568 following the protocol described previously (Duan et al., 2014). Briefly, Arabidopsis
569 seedlings were germinated grown vertically on 0.25xMS media plates for seven days at
570 normal (20ºC) or elevated (30ºC) temperatures. Plates were bathed with five ml of 50
571 uM in H_2DCF-DA (Sigma-Aldrich) suspended in 0.25xMS liquid media for 5 min,
572 followed by two gentle washes with 10 ml of 0.25xMS. Fluorescence images were
573 collected with a Zeiss Axio Imager Z1 fluorescence microscope with 2.5x objective and

574 green (GFP) filter set.

575

576 **Effect of RALF1 peptide on root hair and root growth inhibition**

577 Synthetic Arabidopsis RALF1 polypeptide was synthesized by using 9-fluorenylmethyl
578 chloroformate solid-phase chemistry with a peptide synthesizer from Thermo Scientific
579 company and confirmed by MALD-TOF analysis (Applied Biosystems Voyager System
580 2098, USA). After synthesis, 5 mg of reduced synthetic polypeptide was oxidized by
581 dissolving in 25 ml of degassed 0.1 M ammonium bicarbonate and incubating for 2 days
582 in an opened flask under 4˚C, then lyophilized. Lyophilized RALF1 powder was re-
583 suspended in 10 ml of PBS buffer followed by two buffer exchange steps using Amicon
584 Ultra centrifugal filter (Ultracel-3K, 3000g for 45 min each) to remove any residual
585 ammonium bicarbonate. Seedling germination was performed in 0.5xMS liquid medium
586 at 20ºC for 3 days in long-day conditions (16-h days with 150 $\mu E \cdot m^{-2} \cdot s^{-1}$ (E, Einstein; 1
587 E = 1 mol of photons) light intensity. After 3 days, germinated Arabidopsis seeds were
588 transferred to 6 well Falcon tissue culture plate with 3 ml of 1/2xMS liquid media
589 containing 1 μM RALF1 or an equal volume of PBS and agitated on a shaker at 100 rpm
590 (Model VS2010, Vision Scientific CO.,LTD) for an additional 3 days at 20ºC or 30ºC.
591 All solutions were filter-sterilized (0.2 μm pores, Minisart 16534), and the seedlings were
592 photographed 3 days after being transferred to the media. Quantification of primary root
593 length was measured using ImageJ software. Time-lapse video microscopic analysis was
594 carried out under permissive temperature conditions in wild-type. 0.25x MS liquid media
595 with/without 1 μM RALF1 peptide were pumped to the chamber while imaging. All
596 solutions were filter-sterilized (0.2 μm pores, Minisart 16534).

597

598 **Accession numbers**

599 Sequences of the genes in this paper may be found in the GeneBank/EMBL database
600 library under the following accession numbers: At3g51550 (FER), At4g39990 (RabA4b),
601 At3g18780 (Actin2), At3g04690 (ANX1), At5g28680 (ANX2), At3g46290 (HERK1),
602 At1g30570 (HERK2), At5g54380 (THE1), NP_001085212.1 (*X. laevis* Malectin),
603 NP_055545.1 (*H. sapiens* Malectin).

604

605 ## ACKNOWLEDGEMENTS

606 We thank to Dr. Hen-Ming Wu and Dr. Alice Cheung (University of Massachusetts) for
607 providing *fer-4* and *fer-5* mutants, and Jiyuan Yang for assistance in assembling and
608 editing the manuscript. This research was supported by the U.S. Department of Energy
609 Office of Science, Office of Basic Energy Sciences, Physical Biosciences program (DE-
610 FG02-07ER15887; S.P., F.G., J.C., and E.N,), the National Science Foundation under
611 Grant No. 1817697 (A.A., H.M, and E.N.), and the BK21plus program of the Ministry of
612 Education, Science and Technology in Korea (D.K., and J-D.B.). This work used the
613 Extreme Science and Engineering Discovery Environment (XSEDE; (John W Towns,
614 2014), which is supported by National Science Foundation grant number ACI-1548562.

615

616 ## FIGURE LEGENDS

617 **Figure 1.** Isolation of a temperature-sensitive root hair growth defect mutant.

618 (a) Seven day-old seedling plants were grown vertically in 1/4 MS media under 20˚C and

619 transferred to 30˚C for 6 h, followed by 24 h recovery at 20ºC. Bright field images were
620 collected with a Nikon Eclipse E600 wide-field microscope with a 10x Plan Apo DIC
621 (0.75 NA) lens. Dashed lines indicate root tip positions when seedling plants were
622 transferred to 30˚C condition for 6 hours, and again when they were transferred back to
623 20˚C. Scale bars = 200 µm. (b) Localization of EYFP-RabA4b protein in growing root-
624 hair cells of *fer-ts* mutants at 20˚C and 30˚C. Medial root hair sections were collected
625 using spinning-disk confocal microscopy from growing root-hair cells of seven-day-old
626 seedlings stably expressing EYFP-RabA4b in the *fer-ts* mutant in 20ºC (left) or 30ºC
627 (right) using a Zeiss 40x Plan-Apochromat (1.3 NA) lens and appropriate EYFP
628 fluorescence filter sets. Scale bars = 10 µm. Insets, magnified images to show details of
629 EYFP-RabA4b subcellular localization in root-hair tips. Scale bars = 2 µm. (c)
630 Quantification of root hair length in WT and *fer-ts* mutants under 20˚C (wild-type (n=392),
631 *fer-ts* (n=454)) and 30˚C (wild-type (n=185), *fer-ts* (n=23)) conditions. (d) Calculation of
632 root hair densities in WT and *fer-ts* mutants at 20˚C (wild-type (n=392), *fer-ts* (n=454))
633 and 30˚C (wild-type (n=185), *fer-ts* (n=23)) in fully expanded primary roots of seven-day
634 old plants. In each case, root hair lengths and densities were measured from n=20
635 individual seedlings. Error bars represent SD. **p<0.001 by Student's *t*-test.
636
637 **Figure 2.** Root hair growth dynamics in WT and *fer-ts* seedlings.
638 (a) Root hair tip-growth in WT and *fer-ts* mutant plants under normal (20ºC) and elevated
639 (30ºC) temperatures by time-lapse microscopy. Bright field images of growing root hairs
640 of WT and *fer-ts* mutant plants were collected every minute by time-lapse microscopy
641 using a Zeiss 40x Plan-Apochromat (1.3 NA) lens. Representative images of WT and *fer-*
642 *ts* mutant root hair elongation are presented at 10 min intervals. (b) Quantitative analysis

643 of WT (n=4) and *fer-ts* mutant (n=4) root hair lengths upon transition to 30˚C. WT (black
644 squares) and *fer-ts* (black triangles) mutant root hair elongation were measured every five
645 minutes and root hair lengths were determined using the measure function in Image J.
646 The dashed line indicates transition from 20ºC to 30ºC. Error bars represent SD. *$p<0.05$,
647 **$p<0.01$ by Student's *t*-test.
648

649 **Figure 3.** Temperature-sensitive subcellular dynamics of EYFP-RabA4b labeled
650 compartments in growing root hairs in *fer-ts* mutants.
651 (a) Localization of EYFP-RabA4b protein in a growing root-hair cells of wild-type and
652 *fer-ts* mutant plants at normal (20ºC) or elevated (30ºC) temperature conditions. Growing
653 wild-type and *fer-ts* root hairs were imaged at one minute intervals for 30 min at 20˚C at
654 which the growth chamber temperature was raised to 30˚C. For each time point, both
655 bright field (Bright) and fluorescence (YFP) images were collected sequentially, and tip-
656 localized EYFP-RabA4b compartments were monitored by spinning-disk fluorescence
657 confocal microscopy using a Zeiss 40x Plan-Apochromat (1.3 NA) lens with appropriate
658 EYFP fluorescence filter sets. The grey box indicates when the temperature was raised to
659 30˚C. Quantification of root hair elongation and EYFP-RabA4b root hair tip localization
660 in wild-type (b) and *fer-ts* mutant (c) plants. Root hair length and EYFP-RabA4b
661 fluorescence were quantified by Image J every 1 min.
662

663 **Figure 4.** Map-based cloning of *fer-ts*.
664 (a) A linear diagram of the Arabidopsis third chromosome is shown, with a magnified
665 F24M12 marker region displayed below. The centromere is indicated with filled-rectangle.

666 Low-resolution map-based cloning resulted in identification of the *fer-ts* locus within an
667 approximately 2 Mb region of chromosome III bounded by markers NIT1.2 and CIW19
668 (Double headed arrow). (b) SNPs specific to the ts-mutant within this region were
669 identified using whole genomic resequencing, followed by targeted resequencing of
670 genomic DNA sequencing of *fer-ts* and wild-type parental lines. A single G→A
671 substitution was found in *FERONIA* (At3g51550). The arrowhead indicates G121A
672 substituted mutation in *FERONIA* gene locus. (c) Schematic diagram of FERONIA
673 protein domains and mutation regions, composed of an N-terminal extracellular domain
674 (tandem repeat malectin-like domains; ML1 and ML2), TM (transmembrane) domain in
675 the middle region and a C-terminal kinase domain (serine/threonine kinase), end of N-
676 terminus has signal peptide (SP) sequence for plasma-membrane trafficking. The *fer-4*
677 and *fer-5* mutants displayed that T-DNA was inserted in malectin-like domain 1 and
678 kinase domain, respectively. (d) RT-PCR analysis of T-DNA inserted mutants and EMS
679 mutants. The FER(K) and FER(ExDo) domains were amplified using P1 and P2 primers
680 and P3 and P4 primers, respectively. Actin was used as a loading control.
681

682 **Figure 5.** Localization of the highly conserved glycine mutation in fer-ts in *A. thaliana*
683 FERONIA:RALF23:LLG2 and *X. laevis* malectin structures.
684 (a)Several residues important for binding carbohydrate ligands are conserved in plant
685 CrRLK1L receptor kinase family members. Sequences analyzed include animal
686 Malectin (*X. laevis* and *H. sapiens*) FERONIA and other well-characterized CrRLK1L
687 homologs in *A. thaliana* (ANXUR1; ANX1, ANXUR1; ANX2, HERCULES1; HERK1
688 and THESEUS1; THE1). Putative N-terminal signal peptides are indicated as black

689 dashed lines, and malectin and CrRLK1L ML1 domains by solid lines, respectively. The
690 highly conserved G41 of FER is marked by arrowhead. Black boxes indicate fully
691 conserved residues; shaded boxes indicate similar and partially conserved residues.
692 Conserved residues that have been shown to participate in binding nigerose in the *X.laevis*
693 malectin structure are marked by asterisks. Sequence alignment analysis was performed
694 by CLUSTAL Omega program (http://www.ebi.ac.uk/Tools/msa/clustalo/) and displayed
695 by using BOXSHADE software (www.ch.embnet.org/software/BOX_form.html). (b)
696 Crystal structure of the *X. laevis* malectin protein (PDB ID: 2K46) with binding pocket
697 aromatic residues and the highly conserved glycine residue based on sequence similarity
698 to FER shown in red. (c) Crystal structure of FER protein (green) in complex with
699 RALF23 ligand (magenta) and GPI-anchored protein LLG2 (blue) (PDB ID: 6A5E). No
700 analogous binding pocket is observed on the ML1 domain, as all conserved aromatic
701 residues (red) are buried within the protein. Both (b and c) were generated using PyMol
702 (DeLano Scientific).
703
704 **Figure 6.** The *fer-ts* mutant confers ts-root hair growth defects when crossed with *fer-4*
705 and *fer-5* mutants.
706 (a) Wild-type (WT), *fer-4, fer-5*, and F1 progeny from crosses (paternal = *fer-ts*, maternal
707 = *fer-4* or *fer-5*) of *fer-ts/fer-4* and *fer-ts/fer-5* were grown vertically for seven days at
708 20ºC, transferred to 30ºC for 6 h, and then grown for an additional 24 h at 20ºC. Both
709 *fer-ts/fer-4* and *fer-ts/fer-5* progeny clearly demonstrated a ts-dependent root hair
710 phenotype. Scale bars = 200 µm. (b) Schematic diagram of the *FERONIA* gene structure.
711 Open and filled boxes indicate untranslated regions (UTRs) and exon regions,
712 respectively. The locations of T-DNA insertion mutants (*fer-4* and *fer-5*) and *fer-ts* are

713 indicated by triangles and arrows, respectively. (c) Genotyping of crossed F1 plants.
714 Genomic DNA was extracted from F1 generation plants and subjected PCR to confirm
715 presence of the *fer-4* and *fer-5* genotypes (d) Both *fer-4* and *fer-5* display temperature-
716 dependent root hair phenotypes when transformed with a fluorescently-tagged FER
717 construct containing the *fer-ts* mutation (pFER-FER(G41S)-EYFP). Seven-day old
718 seedlings stably transformed and homozygous for (pFER-EYFP(G41S)-EYFP) were
719 grown vertically at 20ºC, transferred to 30ºC for 6 h, and then grown for an additional 24
720 h at 20ºC. Presence of the transgenic pFER-FER(G41S)-EYFP construct clearly
721 demonstrated a ts-dependent root hair phenotype. Scale bars = 200 µm. (e) Temperature
722 sensitive root hair growth defects of *fer-ts* are fully rescued when transformed with a
723 fluorescently-tagged FER construct (pFER-FER(WT)-EYFP). Seven-day old seedlings
724 stably transformed and homozygous for (pFER-EYFP(WT)-EYFP)were grown vertically
725 at 20ºC, transferred to 30ºC for 6 h, and then grown for an additional 24 h at 20ºC. Bright
726 field images were collected with a Nikon Eclipse E600 wide-field microscope with a 10x
727 Plan Apo DIC (0.75 NA) lens. (f) Subcellular localization of FER(WT)-EYFP protein in
728 roots and root hairs in a rescued *fer-ts* mutant plant. Fluorescent confocal images
729 displaying the subcellular distribution of FER(WT)-EYFP protein was detected from
730 growing root, and mature root hair cells of seven-day-old *fer-ts* seedlings stably
731 transformed and homozygous for pFER-FER(WT)-EYFP. Cells were counter-stained by
732 incubating for 5 min in a FM4-64 to visualize cell membranes. Images were collected
733 by spinning-disk fluorescence confocal microscopy using a Zeiss 40x Plan-Apochromat
734 (1.3 NA) lens with appropriate EYFP and FM4-64 fluorescence filter sets. Scale bars =
735 20 µm.
736

737 **Figure 7.** Subcellular localization of FER(WT)-EYFP and FER(G41S)-EYFP fluorescent
738 fusion proteins in stably transformed *Arabidopsis*.
739 (a) Subcellular localization of FER(WT)-EYFP protein in various tissues. Fluorescent
740 confocal images displaying the subcellular distribution of FER(WT)-EYFP protein was
741 detected from growing root, leaf and root hair cells of seven-day-old seedlings in *pFER-*
742 *FER(WT)-EYFP*/WT transgenic plants. Cell walls were counter-stained by incubating for
743 5 min in a propidium iodide (PI) solution (10 μg/ml). Images were collected by
744 spinning-disk fluorescence confocal microscopy using a Zeiss 40x Plan-Apochromat (1.3
745 NA) lens with appropriate EYFP and PI fluorescence filter sets. Scale bars = 20 μm. (b)
746 Magnified images of FER(WT)-EYFP fluorescence. FER(WT)-EYFP in wild-type of
747 growing root cells of seven-day-old *A. thaliana* seedlings was detected by spinning-disc
748 confocal microscopy using a Zeiss 100x Plan-Apochromat (1.46 NA) oil immersion
749 objective with appropriate EYFP and PI filter sets. Scale bars = 10 μm. (c-d) Subcellular
750 localization of FER(WT)-EYFP (c) and FER(G41S)-EYFP (d) fluorescent fusions in root
751 and root hair cells at normal (20°C) and elevated (30°C) temperatures. Cells from *fer-4*
752 plants stably transformed and homozygous for FER(WT)-EYFP or FER(G41S)-EYFP
753 were counterstained with FM4-64 (5 μM) for five minutes to visualize cell membranes.
754 Images were collected by spinning-disk fluorescence confocal microscopy using a Zeiss
755 40x Plan-Apochromat (1.3 NA) lens with appropriate EYFP and FM4-64 fluorescence
756 filter sets. Scale bars = 20 μm; root, 10 μm; root hair.
757
758 **Figure 8.** Subcellular localization dynamics of FER(WT)-EYFP and FER(G41S)-EYFP
759 proteins in growing root hair cells under both normal (20°C) and elevated (30°C)
760 temperatures.

761 (a) Root hair tip-growth in stably transformed lines expressing FER(WT)-EYFP and
762 FER(G41S)-EYFP fluorescent fusion proteins under (20°C) and (30°C) temperature by
763 time-lapse microscopy. Confocal images of were acquired using a Leica confocal laser-
764 scanning microscope SP8 with a 63x oil lens (Numerical Aperture = 1.4) with 5s intervals.
765 Representative images are presented at 50s intervals (10 frames). Scale bar: 10 μm. (b)
766 Schematic diagram shown areas and lines used for fluorescence intensity quantification.
767 Apical (red line) and peripheral (blue line) plasma membrane domains were measured,
768 and the area between the apical plasma membrane and green line represents the vesicle-
769 rich zone. (c) Quantitative analysis of root hair growth in stably transformed lines
770 expressing FER(WT)-EYFP (n=3) and FER(G41S)-EYFP (n=3). Root hair elongation
771 was measured every 50s using the measurement function in ImageJ. (d) Quantitative
772 analysis of YFP intensity of vesicle-rich zone. (e) Quantitative analysis of YFP intensity
773 of apical/ peripheral ratio. Values are normalized using 0s as 100%. The dashed line
774 indicates time point of transition from permissive (20°C) to (30°C). Error bars in (c, d, e)
775 represent SD. (f) Protein turnover rates of FER(WT)-EYFP and FER(G41S)-EYFP at
776 elevated temperature (30°C). Five-day old seedling were grown at 20°C and then treated
777 with 200 μM cycloheximide and transferred to 30°C. Total proteins were extracted at
778 each time point and the relative levels were determined using immunoblotting with anti-
779 GFP and anti-actin antibodies. FER(G41S)-EYFP levels rapidly decreased during the
780 time course, while levels of FER(WT)-EYFP were not significantly reduced. Actin was
781 used as a loading control.
782
783 **Figure 9.** RALF peptide treatment terminates root hair growth in FER(WT)-EYFP

784 expressing line.

785 (a) Root hair tip-growth in stably transformed lines expressing FER(WT)-EYFP

786 fluorescent fusion protein under permissive (20°C) temperature by time-lapse microscopy.

787 Bright field images of growing root hair cells (n=3) were collected using a Nikon Eclipse

788 E600 wide-field microscope with a x 20 Plan Apo (0.45 NA) lens with 5s intervals. The

789 dashed line represents when media containing RALF1 (1 μM) was perfused into the

790 growth chamber. Representative images are presented at 200s intervals. Scale bar: 50

791 μm. (b) Quantification of root hair growth. Root hair elongation was measured every 50s

792 using the measurement function in ImageJ. Error bars represent SD.

793

794 **Figure 10**. *fer-ts* mutants are partially insensitive to RALF1 peptide mediated root growth

795 inhibition at elevated temperatures.

796 Wild-type (WT), *fer-ts*, or *fer-5* plants were germinated and grown for 3 days in ½ MS

797 liquid media at 20ºC, and then transferred to ½ MS liquid media containing 1uM RALF1

798 peptide (RALF+) or a mock buffer control (RALF-) and grown an additional 3 days at

799 20ºC (a) or 30ºC (b). Images of representative seedlings were collected using an Olympus

800 SZX12 stereoscopic microscope. Quantification of primary root lengths (n = 10 seedlings)

801 in the presence or absence of RALF1 peptide treatment in normal, 20˚C (c) and elevated,

802 30˚C (d) conditions. Primary root lengths were determined using Image J. Error bars

803 represent SD. *p<0.05, **p<0.01 by Student's *t*-test.

804

805 **Figure 11.** Detection of ROS in WT, *fer-ts* and *fer-5* primary roots and root hairs.

806 (a) ROS accumulation in normal and elevated temperature conditions with or without

807 auxin treatments. Wild-type (WT), *fer-ts*, *fer-4*, or *fer-5* seedlings were grown vertically
808 on ¼ MS media plates for seven days at normal (20ºC) or elevated (30ºC) temperatures
809 in the presence or absence of (10 nM NAA). Plates were bathed with five ml of 50 uM in
810 H_2DCF-DA suspended in ¼ MS liquid media for 5 min, followed by two gentle washes
811 with 10 ml of ¼ MS. Fluorescence images were collected with a Zeiss Axio Imager Z1
812 fluorescence microscope with 2.5x objective and green (GFP) filter set. The WT ROS
813 image was acquired by auto-exposure, all other images were acquired using the WT
814 exposure conditions. Scale bars = 500 µm. (b) The rectangle in (a) indicates a
815 representative region of interest (ROI) where average ROS intensity was quantified for
816 the samples. Intensities of ROS were quantified by image J program. Error bars represent
817 SD. **p<0.01 by Student's *t*-test.
818

819 **SUPPORTING INFORMATION**

820 Additional supporting Information may be found in the online version of this article.
821 **Figure S1.** Primary root growth of *fer-ts* mutants under normal and elevated temperature
822 conditions. (a) Photographs of wild-type and *ltl2* mutant under permissive and non-
823 permissive temperature conditions. (b) Measurements of primary root growth length
824 under normal (20ºC) and elevated (30ºC) temperature conditions. (c) Primary root growth
825 rate under 20˚C and 30˚C conditions. (a)-(c) Seven day-old wild-type (WT; n=25) and
826 *fer-ts* (n=25) seedlings were transferred to the 30˚C for two weeks and primary roots were
827 scanned by EPSON 4990 photo scanner every second day. The primary roots length were
828 determined using Image J, and root growth rates were calculated by dividing growth by
829 48 hours (mm/h). Error bars represent SD. *p<0.05 by Student's *t*-test.
830

831 **Figure S2.** Root hair growth chamber temperature measurement during transition from
832 normal (20°C) to elevated (30°C) temperature conditions.
833
834 **Figure S3.** Sequence alignment of *Arabidopsis* CrRLK1L subfamily receptor kinases.
835 Multiple-sequence alignment analysis was performed with the Clustal Omega program
836 (http://www.ebi.ac.uk/Tools/msa/clustalo/) and displayed using BOXSHADE
837 (www.ch.embnet.org/software/BOX_form.html). Sequence similarity analysis of CrRLK
838 subfamily members in Arabidopsis. *At3g51550* encodes FERONIA protein. The highly
839 conserved FERONIA G41 and additional putative key residues are marked by black
840 arrowheads and asterisks, respectively. Black boxes indicate conserved residues; shaded
841 boxes indicate residues with conserved substitutions.
842
843 **Figure S4.** Temperature-sensitive root hair growth in *fer-ts/fer-4* and *fer-ts/fer-5* F1 plants.
844 (a) Wild-type (WT), *fer-4, fer-5*, and F1 progeny from crosses (maternal = *fer-ts*, paternal
845 = *fer-4* or *fer-5*) of *fer-ts/fer-4* and *fer-ts/fer-5* were grown vertically for seven days at
846 20°C, transferred to 30°C for 6 h, and then grown for an additional 24 h at 20°C. Both
847 *fer-ts/fer-4* and *fer-ts/fer-5* progeny clearly demonstrated a ts-dependent root hair
848 phenotype. Scale bars = 200 µm. (b) Genotyping of crossed F1 plants. Genomic DNA
849 was extracted from F1 generation plants and subjected PCR to confirm presence of the
850 *fer-4* and *fer-5* genotypes.
851
852 **Figure S5.** In elevated temperatures, *fer-ts* responds to hormone treatments similarly to
853 *fer-4* and *fer-5* mutants.
854 (a and b) Quantification of root hair length and density in normal (upper panels) and

855 elevated temperature (lower panels) in 10, 100, and 1000 uM concentrations for each of
856 the various hormone treatments (NAA; Auxin, ACC; ethylene, Kinetin; Cytokinin, ABA;
857 Abscisic acid, eBL; epi-brassinosteroid, MeJA; methyl jasmonic acid, SA; Salicylic acid).
858 Three-day-old seedlings were transferred into ½ MS liquid media containing three
859 different concentrations of the various hormones. Then, transferred plants were incubated
860 at 20˚C and 30˚C for seven days before quantification. The root hairs were photographed
861 by Olympus AX-70 microscope and root hair length and densities were determined by
862 image J. Error bars represent SD.
863
864 **Figure S6.** Hormonal effects on primary root length, total lateral root number, fresh
865 weight and total leaf number in normal and elevated temperature conditions for *fer-ts*,
866 *fer-4*, and *fer-5* plants. Primary root length (a), lateral root number (b), fresh weight (c),
867 and leaf number (d) were measured in normal (upper panels) and elevated (lower panels)
868 temperatures in 10, 100, and 1000 uM concentrations for each of the various hormone
869 treatments (NAA; Auxin, ACC; ethylene, Kinetin; Cytokinin, ABA; Abscisic acid, eBL;
870 epi-brassinosteroid, MeJA; methyl jasmonic acid, SA; Salicylic acid). Three-day-old
871 seedlings (n=20 each for wild-type, *fer-ts*, *fer-4*, and *fer-5*) were transferred into ½ MS
872 liquid media containing three different concentrations of the various hormones. Then,
873 transferred plants were incubated at 20˚C and 30˚C for seven days before quantification.
874 Error bars represent SD.
875
876 **Movie S1.** Time-lapse imaging of growing root hair of WT and *fer-ts* mutants during
877 permissive and non-permissive temperatures. The root hair growth of WT and *fer-ts* plants
878 (seven day-old seedlings) mounted in a temperature-controlled perfusion chamber were

879 imaged with a Nikon ECLIPSE E600 microscopy with a 10x Plan Apo (0.45 NA) lens.
880 Perfused plant growth chamber temperatures were controlled by a combination of a dry
881 air thermostat linked to a single channel Automatic Temperature Controller TC-324B, and
882 real-time measurement using an Infrared Thermometer IRT0421. Images of WT and *fer-*
883 *ts* mutant root hairs were collected every five seconds and cropped by Photoshop
884 Lightroom version 5.3. Video clips were constructed by VEGAS 6.0 program from Sony
885 (30 frames/s).
886
887 **Movie S2.** Dynamics of YFP fused FERONIA protein localization in growing root hair.
888 The growing root hair of YFP fused FERONIA protein (seven day-old seedlings) using
889 perfusion chambers was observed by Zeiss Observer.A1 laser confocal microscopy
890 connected to a CSU10 confocal scanner unit (Yokogawa, Japan) and a 63x Plan-
891 Apochromat (1.40 NA) oil objective with 491 nm laser excitation and a 535 nm emission
892 filter for EYFP fluorescence. Images were collected with a Hamamatsu C9100-50 camera
893 and operated using the Volocity software version 5. Time-lapse fluorescent images were
894 taken every 5 s for 20 min and automatically constructed by Volocity software version 5
895 (30 frames/s).
896
897 **Movie S3.** FER(WT)-EYFP and FER(G41S)-EYFP protein localization in root hairs at
898 normal (20ºC) and elevated (30ºC) temperature conditions.
899 Subcellular localization of pFER-FER(WT)-EYFP and pFER-FER(G41S)-EYFP fusion
900 proteins in root hair cells of seven-day-old seedlings were collected ever 5 s for 350 s at
901 20˚C at which point the perfusion chamber was transferred to 30˚C for an additional 300
902 s. Perfused plant growth chamber temperatures were controlled by a combination of a dry

903 air thermostat linked to a single channel Automatic Temperature Controller TC-324B, and
904 real-time measurement using an Infrared Thermometer IRT0421. Confocal images were
905 collected YFP signal were acquired using a Leica confocal laser-scanning microscope
906 SP8 with a 63x oil lens (1.4 NA). Movies were constructed using ImageJ (20 frames/s).
907
908 **Movie S4.** Effect of RALF1 peptide on root hair growth. Bright-field images of root hair
909 cells of seven-day-old seedlings in a stably-transformed *fer-4* line expressing FER(WT)-
910 EYFP were imaged using a Nikon Eclipse E600 wide-field microscope with a 10x Plan
911 Apo (0.45 NA) lens. Time-lapse images were collected every 5 s for 20 min at 20ºC in
912 0.25xMS media, at which point the perfusion buffer was switched to 0.25xMS media with
913 1 μM RALF1 peptide. Movies were constructed using ImageJ (20 frames/s).
914
915 **Table S1. List of primers used in this study.**
916

917 # REFERENCES

918 **Bell CJ, Ecker JR** (1994) Assignment of 30 microsatellite loci to the linkage map of
919 Arabidopsis. Genomics **19:** 137-144

920 **Boisson-Dernier A, Roy S, Kritsas K, Grobei MA, Jaciubek M, Schroeder JI,**
921 **Grossniklaus U** (2009) Disruption of the pollen-expressed FERONIA homologs
922 ANXUR1 and ANXUR2 triggers pollen tube discharge. Development **136:** 3279-
923 3288

924 **Carol RJ, Dolan L** (2006) The role of reactive oxygen species in cell growth: lessons
925 from root hairs. J Exp Bot **57:** 1829-1834

926 **Chen J, Yu F, Liu Y, Du C, Li X, Zhu S, Wang X, Lan W, Rodriguez PL, Liu X, Li**
927 **D, Chen L, Luan S** (2016) FERONIA interacts with ABI2-type phosphatases to
928 facilitate signaling cross-talk between abscisic acid and RALF peptide in
929 Arabidopsis. Proc Natl Acad Sci U S A **113:** E5519-5527

930 **Cheung AY, Wu HM** (2011) THESEUS 1, FERONIA and relatives: a family of cell wall-
931 sensing receptor kinases? Curr Opin Plant Biol **14:** 632-641

932 **Cho HT, Cosgrove DJ** (2002) Regulation of root hair initiation and expansin gene
933 expression in Arabidopsis. Plant Cell **14:** 3237-3253

934 **Clough SJ, Bent AF** (1998) Floral dip: a simplified method for Agrobacterium-mediated
935 transformation of Arabidopsis thaliana. Plant J **16:** 735-743

936 **Cole RA, Fowler JE** (2006) Polarized growth: maintaining focus on the tip. Curr Opin
937 Plant Biol **9:** 579-588

938 **Deslauriers SD, Larsen PB** (2010) FERONIA is a key modulator of brassinosteroid and
939 ethylene responsiveness in Arabidopsis hypocotyls. Mol Plant **3:** 626-640

940 **Du S, Qu LJ, Xiao J** (2018) Crystal structures of the extracellular domains of the
941 CrRLK1L receptor-like kinases ANXUR1 and ANXUR2. Protein Sci **27:** 886-892

942 **Duan Q, Kita D, Johnson EA, Aggarwal M, Gates L, Wu HM, Cheung AY** (2014)
943 Reactive oxygen species mediate pollen tube rupture to release sperm for
944 fertilization in Arabidopsis. Nat Commun **5:** 3129

945 **Duan Q, Kita D, Li C, Cheung AY, Wu HM** (2010) FERONIA receptor-like kinase
946 regulates RHO GTPase signaling of root hair development. Proc Natl Acad Sci U
947 S A **107:** 17821-17826

948 **Duan Q, Liu MJ, Kita D, Jordan SS, Yeh FJ, Yvon R, Carpenter H, Federico AN,**
949 **Garcia-Valencia LE, Eyles SJ, Wang CS, Wu HM, Cheung AY** (2020)
950 FERONIA controls pectin- and nitric oxide-mediated male-female interaction.
951 Nature **579:** 561-566
952 **Escobar-Restrepo JM, Huck N, Kessler S, Gagliardini V, Gheyselinck J, Yang WC,**
953 **Grossniklaus U** (2007) The FERONIA receptor-like kinase mediates male-
954 female interactions during pollen tube reception. Science **317:** 656-660
955 **Feng W, Kita D, Peaucelle A, Cartwright HN, Doan V, Duan Q, Liu MC, Maman J,**
956 **Steinhorst L, Schmitz-Thom I, Yvon R, Kudla J, Wu HM, Cheung AY,**
957 **Dinneny JR** (2018) The FERONIA Receptor Kinase Maintains Cell-Wall
958 Integrity during Salt Stress through Ca(2+) Signaling. Curr Biol **28:** 666-675 e665
959 **Foreman J, Demidchik V, Bothwell JHF, Mylona P, Miedema H, Torres MA,**
960 **Linstead P, Costa S, Brownlee C, Jones JDG, Davies JM, Dolan L** (2003)
961 Reactive oxygen species produced by NADPH oxidase regulate plant cell growth.
962 Nature **422:** 442-446
963 **Ge Z, Bergonci T, Zhao Y, Zou Y, Du S, Liu MC, Luo X, Ruan H, Garcia-Valencia**
964 **LE, Zhong S, Hou S, Huang Q, Lai L, Moura DS, Gu H, Dong J, Wu HM,**
965 **Dresselhaus T, Xiao J, Cheung AY, Qu LJ** (2017) Arabidopsis pollen tube
966 integrity and sperm release are regulated by RALF-mediated signaling. Science
967 **358:** 1596-1600
968 **Gilroy S, Jones DL** (2000) Through form to function: root hair development and nutrient
969 uptake. Trends Plant Sci **5:** 56-60
970 **Gonneau M, Desprez T, Martin M, Doblas VG, Bacete L, Miart F, Sormani R,**
971 **Hematy K, Renou J, Landrein B, Murphy E, Van De Cotte B, Vernhettes S,**
972 **De Smet I, Hofte H** (2018) Receptor Kinase THESEUS1 Is a Rapid
973 Alkalinization Factor 34 Receptor in Arabidopsis. Curr Biol **28:** 2452-2458 e2454
974 **Guo H, Li L, Ye H, Yu X, Algreen A, Yin Y** (2009) Three related receptor-like kinases
975 are required for optimal cell elongation in Arabidopsis thaliana. Proc Natl Acad
976 Sci U S A **106:** 7648-7653
977 **Haruta M, Sabat G, Stecker K, Minkoff BB, Sussman MR** (2014) A peptide hormone
978 and its receptor protein kinase regulate plant cell expansion. Science **343:** 408-
979 411

980 **Hematy K, Hofte H** (2008) Novel receptor kinases involved in growth regulation. Curr
981 Opin Plant Biol **11:** 321-328
982 **Hematy K, Sado PE, Van Tuinen A, Rochange S, Desnos T, Balzergue S, Pelletier S,**
983 **Renou JP, Hofte H** (2007) A receptor-like kinase mediates the response of
984 Arabidopsis cells to the inhibition of cellulose synthesis. Curr Biol **17:** 922-931
985 **Hepler PK, Vidali L, Cheung AY** (2001) Polarized cell growth in higher plants. Annu
986 Rev Cell Dev Biol **17:** 159-187
987 **Huang GQ, Li E, Ge FR, Li S, Wang Q, Zhang CQ, Zhang Y** (2013) Arabidopsis
988 RopGEF4 and RopGEF10 are important for FERONIA-mediated developmental
989 but not environmental regulation of root hair growth. New Phytol **200:** 1089-1101
990 **Huck N, Moore JM, Federer M, Grossniklaus U** (2003) The Arabidopsis mutant
991 feronia disrupts the female gametophytic control of pollen tube reception.
992 Development **130:** 2149-2159
993 **John W Towns TC, Maytal Dahan, Ian Foster, Kelly Gaither, Andrew Grimshaw,**
994 **Victor Hazlewood, Scott Lathrop, Dave Lifka, Gregory D. Peterson, Ralph**
995 **Roskies, J. Ray Scott, Nancy Wilkens-Diehr** (2014) XSEDE: Accelerating
996 scientific discovery. Computing in Science and Engineering **16:** 62-74
997 **Jones MA, Shen JJ, Fu Y, Li H, Yang Z, Grierson CS** (2002) The Arabidopsis Rop2
998 GTPase is a positive regulator of both root hair initiation and tip growth. Plant
999 Cell **14:** 763-776
1000 **Lehti-Shiu MD, Zou C, Hanada K, Shiu SH** (2009) Evolutionary history and stress
1001 regulation of plant receptor-like kinase/pelle genes. Plant Physiol **150:** 12-26
1002 **Li C, Wu HM, Cheung AY** (2016) FERONIA and Her Pals: Functions and Mechanisms.
1003 Plant Physiol **171:** 2379-2392
1004 **Lindner H, Muller LM, Boisson-Dernier A, Grossniklaus U** (2012) CrRLK1L
1005 receptor-like kinases: not just another brick in the wall. Curr Opin Plant Biol **15:**
1006 659-669
1007 **Miyazaki S, Murata T, Sakurai-Ozato N, Kubo M, Demura T, Fukuda H, Hasebe M**
1008 (2009) ANXUR1 and 2, sister genes to FERONIA/SIRENE, are male factors for
1009 coordinated fertilization. Curr Biol **19:** 1327-1331
1010 **Molendijk AJ, Bischoff F, Rajendrakumar CS, Friml J, Braun M, Gilroy S, Palme**
1011 **K** (2001) Arabidopsis thaliana Rop GTPases are localized to tips of root hairs and

control polar growth. Embo J **20:** 2779-2788

Morillo SA, Tax FE (2006) Functional analysis of receptor-like kinases in monocots and dicots. Curr Opin Plant Biol **9:** 460-469

Muller LN, Muhle-Goll C, Biskup MB (2010) The Glc2Man2-fragment of the N-glycan precursor--a novel ligand for the glycan-binding protein malectin? Org Biomol Chem **8:** 3294-3299

Ngo QA, Vogler H, Lituiev DS, Nestorova A, Grossniklaus U (2014) A calcium dialog mediated by the FERONIA signal transduction pathway controls plant sperm delivery. Dev Cell **29:** 491-500

Pearce G, Moura DS, Stratmann J, Ryan CA, Jr. (2001) RALF, a 5-kDa ubiquitous polypeptide in plants, arrests root growth and development. Proc Natl Acad Sci U S A **98:** 12843-12847

Preuss ML, Santos-Serna J, Falbel TG, Bednarek SY, Nielsen E (2004) The Arabidopsis Rab GTPase RabA4b Localizes to the Tips of Growing Root Hair Cells. Plant Cell **16:** 1589-1603

Preuss ML, Schmitz AJ, Thole JM, Bonner HK, Otegui MS, Nielsen E (2006) A role for the RabA4b effector protein PI-4Kbeta1 in polarized expansion of root hair cells in Arabidopsis thaliana. J Cell Biol **172:** 991-998

Rotman N, Rozier F, Boavida L, Dumas C, Berger F, Faure JE (2003) Female control of male gamete delivery during fertilization in Arabidopsis thaliana. Curr Biol **13:** 432-436

Schallus T, Jaeckh C, Feher K, Palma AS, Liu Y, Simpson JC, Mackeen M, Stier G, Gibson TJ, Feizi T, Pieler T, Muhle-Goll C (2008) Malectin: a novel carbohydrate-binding protein of the endoplasmic reticulum and a candidate player in the early steps of protein N-glycosylation. Mol Biol Cell **19:** 3404-3414

Schindelin J, Arganda-Carreras I, Frise E, Kaynig V, Longair M, Pietzsch T, Preibisch S, Rueden C, Saalfeld S, Schmid B, Tinevez JY, White DJ, Hartenstein V, Eliceiri K, Tomancak P, Cardona A (2012) Fiji: an open-source platform for biological-image analysis. Nat Methods **9:** 676-682

Schoenaers S, Balcerowicz D, Breen G, Hill K, Zdanio M, Mouille G, Holman TJ, Oh J, Wilson MH, Nikonorova N, Vu LD, De Smet I, Swarup R, De Vos WH, Pintelon I, Adriaensen D, Grierson C, Bennett MJ, Vissenberg K (2018) The

1044 Auxin-Regulated CrRLK1L Kinase ERULUS Controls Cell Wall Composition
1045 during Root Hair Tip Growth. Curr Biol **28:** 722-732 e726
1046 **Schulze-Muth P, Irmler S, Schroder G, Schroder J** (1996) Novel type of receptor-like
1047 protein kinase from a higher plant (Catharanthus roseus). cDNA, gene,
1048 intramolecular autophosphorylation, and identification of a threonine important
1049 for auto- and substrate phosphorylation. J Biol Chem **271:** 26684-26689
1050 **Shih HW, Miller ND, Dai C, Spalding EP, Monshausen GB** (2014) The receptor-like
1051 kinase FERONIA is required for mechanical signal transduction in Arabidopsis
1052 seedlings. Curr Biol **24:** 1887-1892
1053 **Shiu SH, Bleecker AB** (2001) Plant receptor-like kinase gene family: diversity, function,
1054 and signaling. Sci STKE **2001:** re22
1055 **Shiu SH, Bleecker AB** (2003) Expansion of the receptor-like kinase/Pelle gene family
1056 and receptor-like proteins in Arabidopsis. Plant Physiol **132:** 530-543
1057 **Smith IF, Hitt B, Green KN, Oddo S, LaFerla FM** (2005) Enhanced caffeine-induced
1058 Ca2+ release in the 3xTg-AD mouse model of Alzheimer's disease. J Neurochem
1059 **94:** 1711-1718
1060 **Stegmann M, Monaghan J, Smakowska-Luzan E, Rovenich H, Lehner A, Holton N,**
1061 **Belkhadir Y, Zipfel C** (2017) The receptor kinase FER is a RALF-regulated
1062 scaffold controlling plant immune signaling. Science **355:** 287-289
1063 **Thole JM, Vermeer JE, Zhang Y, Gadella TW, Jr., Nielsen E** (2008) Root hair
1064 defective4 encodes a phosphatidylinositol-4-phosphate phosphatase required for
1065 proper root hair development in Arabidopsis thaliana. Plant Cell **20:** 381-395
1066 **Weigel D, Glazebrook J** (2006) EMS Mutagenesis of Arabidopsis Seed. CSH Protoc
1067 **2006**
1068 **Xiao Y, Stegmann M, Han Z, DeFalco TA, Parys K, Xu L, Belkhadir Y, Zipfel C,**
1069 **Chai J** (2019) Mechanisms of RALF peptide perception by a heterotypic receptor
1070 complex. Nature **572:** 270-274
1071 **Yu F, Li J, Huang Y, Liu L, Li D, Chen L, Luan S** (2014) FERONIA receptor kinase
1072 controls seed size in Arabidopsis thaliana. Mol Plant **7:** 920-922
1073 **Yu F, Qian L, Nibau C, Duan Q, Kita D, Levasseur K, Li X, Lu C, Li H, Hou C, Li**
1074 **L, Buchanan BB, Chen L, Cheung AY, Li D, Luan S** (2012) FERONIA receptor
1075 kinase pathway suppresses abscisic acid signaling in Arabidopsis by activating

1076 ABI2 phosphatase. Proc Natl Acad Sci U S A **109:** 14693-14698
1077

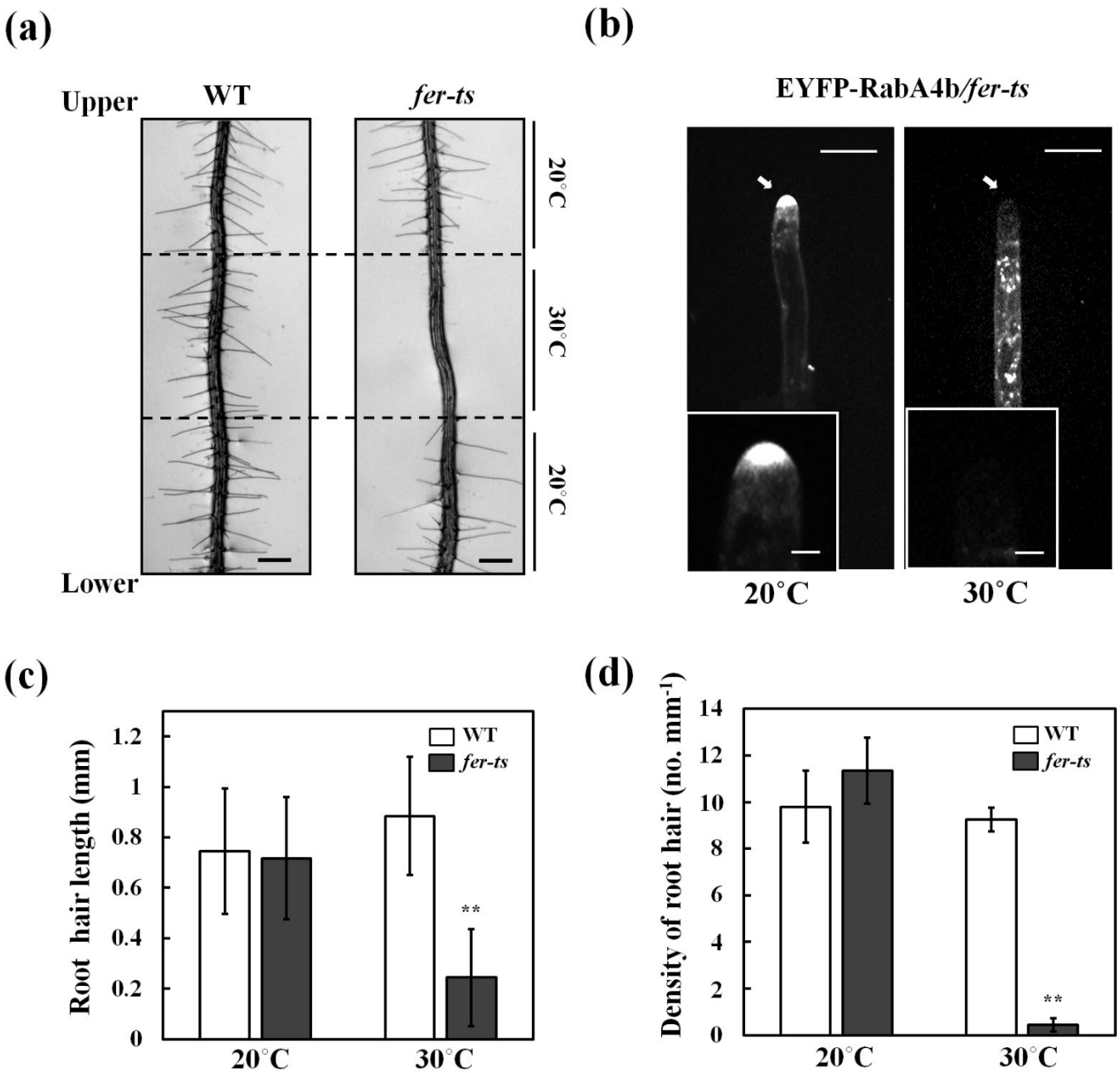

Figure 1. Isolation of a temperature-sensitive root hair growth defect mutant.
(a) Seven day-old seedling plants were grown vertically in 0.25xMS media under 20˚C and transferred to 30˚C for 6 h, followed by 24 h recovery at 20ºC. Bright field images were collected with a Nikon Eclipse E600 wide-field microscope with a 10x Plan Apo DIC (0.75 NA) lens. Dashed lines indicate root tip positions when seedling plants were transferred to 30˚C condition for 6 hours, and again when they were transferred back to 20˚C. Scale bars = 200 µm. (b) Localization of EYFP-RabA4b protein in growing root-hair cells of *fer-ts* mutants at 20˚C and 30˚C. Medial root hair sections were collected using spinning-disk confocal microscopy from growing root-hair cells of seven-day-old seedlings stably expressing EYFP-RabA4b in the *fer-ts* mutant in 20ºC (left) or 30ºC (right) using a Zeiss 40x Plan-Apochromat (1.3 NA) lens and appropriate EYFP fluorescence filter sets. Scale bars = 10 µm. Insets, magnified images to show details of EYFP-RabA4b subcellular localization in root-hair tips. Scale bars = 2 µm. (c) Quantification of root hair length in WT and *fer-ts* mutants under 20˚C (wild-type (n=392), *fer-ts* (n=454)) and 30˚C (wild-type (n=185), *fer-ts* (n=23)) conditions. (d) Calculation of root hair densities in WT and *fer-ts* mutants at 20˚C (wild-type (n=392), *fer-ts* (n=454)) and 30˚C (wild-type (n=185), *fer-ts* (n=23)) in fully expanded primary roots of seven-day old plants. In each case, root hair lengths and densities were measured from n=20 individual seedlings. Error bars represent SD. **p<0.001 by Student's *t*-test.

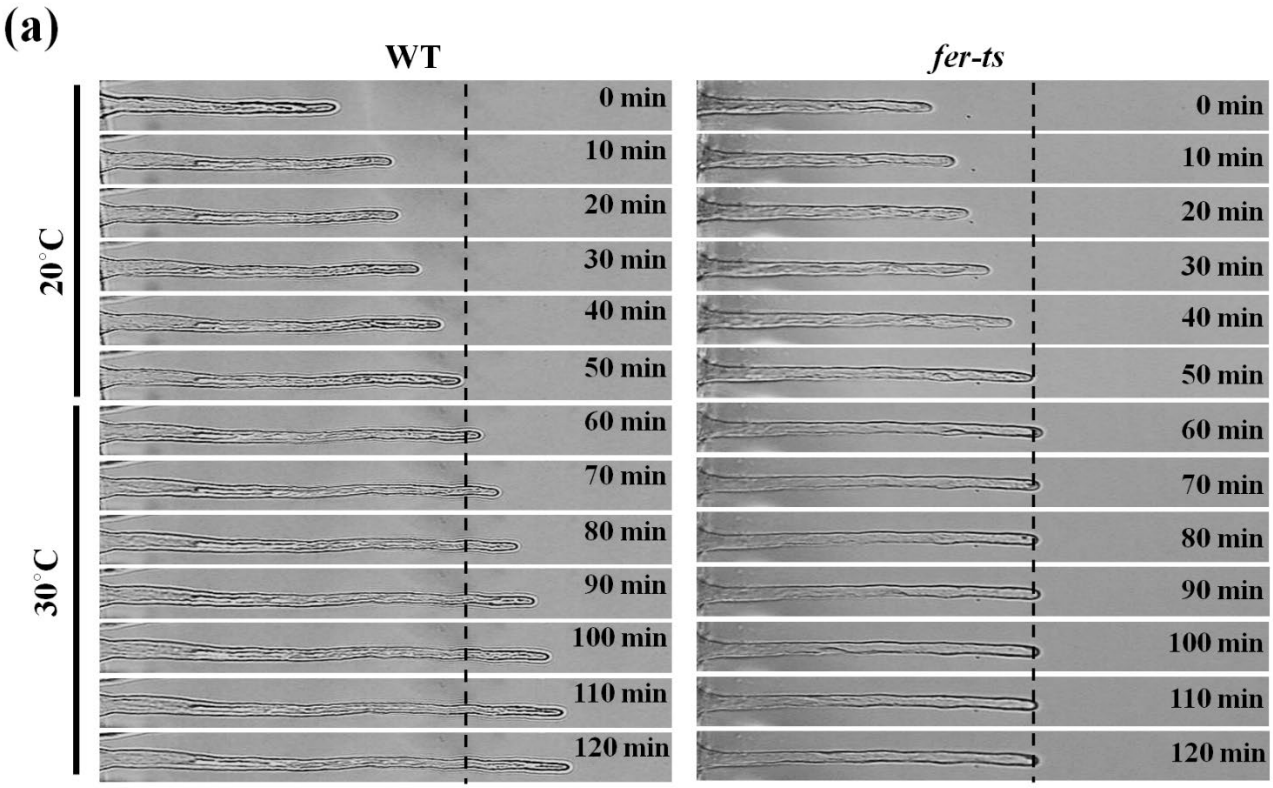

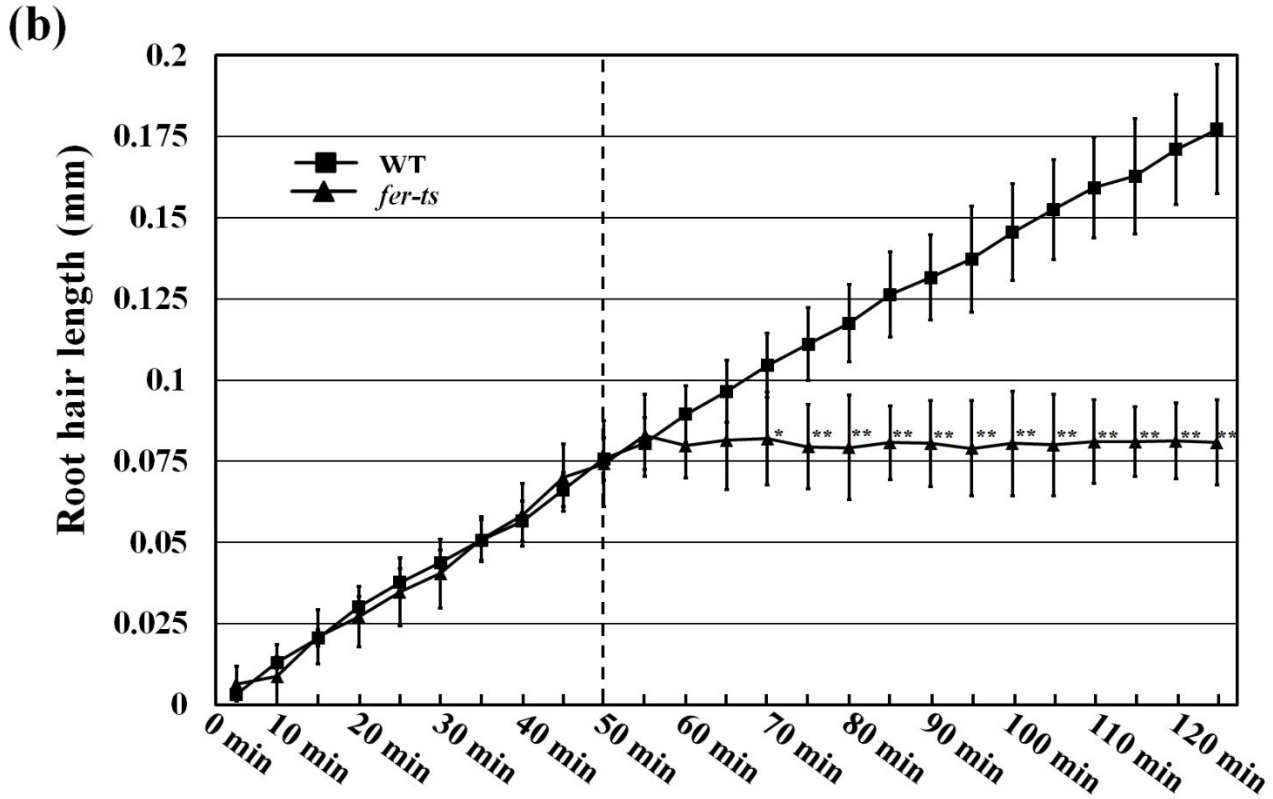

Figure 2. Root hair growth dynamics in WT and *fer-ts* seedlings.(a) Root hair tip-growth in WT and *fer-ts* mutant plants under normal (20ºC) and elevated (30ºC) temperatures by time-lapse microscopy. Bright field images of growing root hairs of WT and *fer-ts* mutant plants were collected every minute by time-lapse microscopy using a Zeiss 40x Plan-Apochromat (1.3 NA) lens. Representative images of WT and *fer-ts* mutant root hair elongation are presented at 10 min intervals. (b) Quantitative analysis of WT (n=4) and *fer-ts* mutant (n=4) root hair lengths upon transition to 30˚C. WT (black squares) and *fer-ts* (black triangles) mutant root hair elongation were measured every five minutes and root hair lengths were determined using the measure function in Image J. The dashed line indicates transition from 20ºC to 30ºC. Error bars represent SD. *$p<0.05$, **$p<0.01$ by Student's *t*-test.

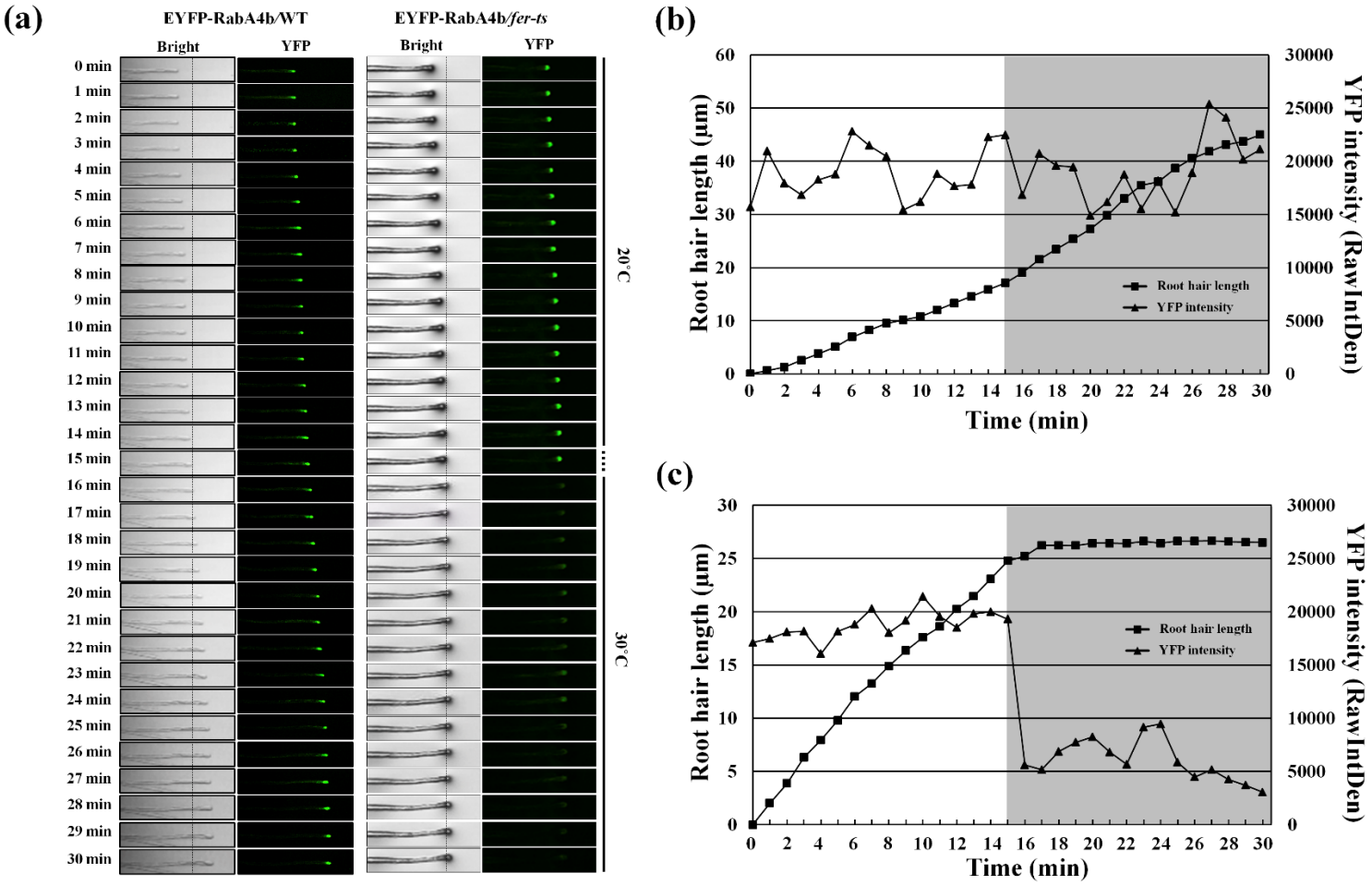

Figure 3. Temperature-sensitive subcellular dynamics of EYFP-RabA4b labeled compartments in growing root hairs in *fer-ts* mutants.

(a) Localization of EYFP-RabA4b protein in a growing root-hair cells of wild-type and *fer-ts* mutant plants at normal (20ºC) or elevated (30ºC) temperature conditions. Growing wild-type and *fer-ts* root hairs were imaged at one minute intervals for 30 min at 20˚C at which the growth chamber temperature was raised to 30˚C. For each time point, both bright field (Bright) and fluorescence (YFP) images were collected sequentially, and tip-localized EYFP-RabA4b compartments were monitored by spinning-disk fluorescence confocal microscopy using a Zeiss 40x Plan-Apochromat (1.3 NA) lens with appropriate EYFP fluorescence filter sets. The grey box indicates when the temperature was raised to 30˚C. Quantification of root hair elongation and EYFP-RabA4b root hair tip localization in wild-type (b) and *fer-ts* mutant (c) plants. Root hair length and EYFP-RabA4b fluorescence were quantified by Image J every 1 min.

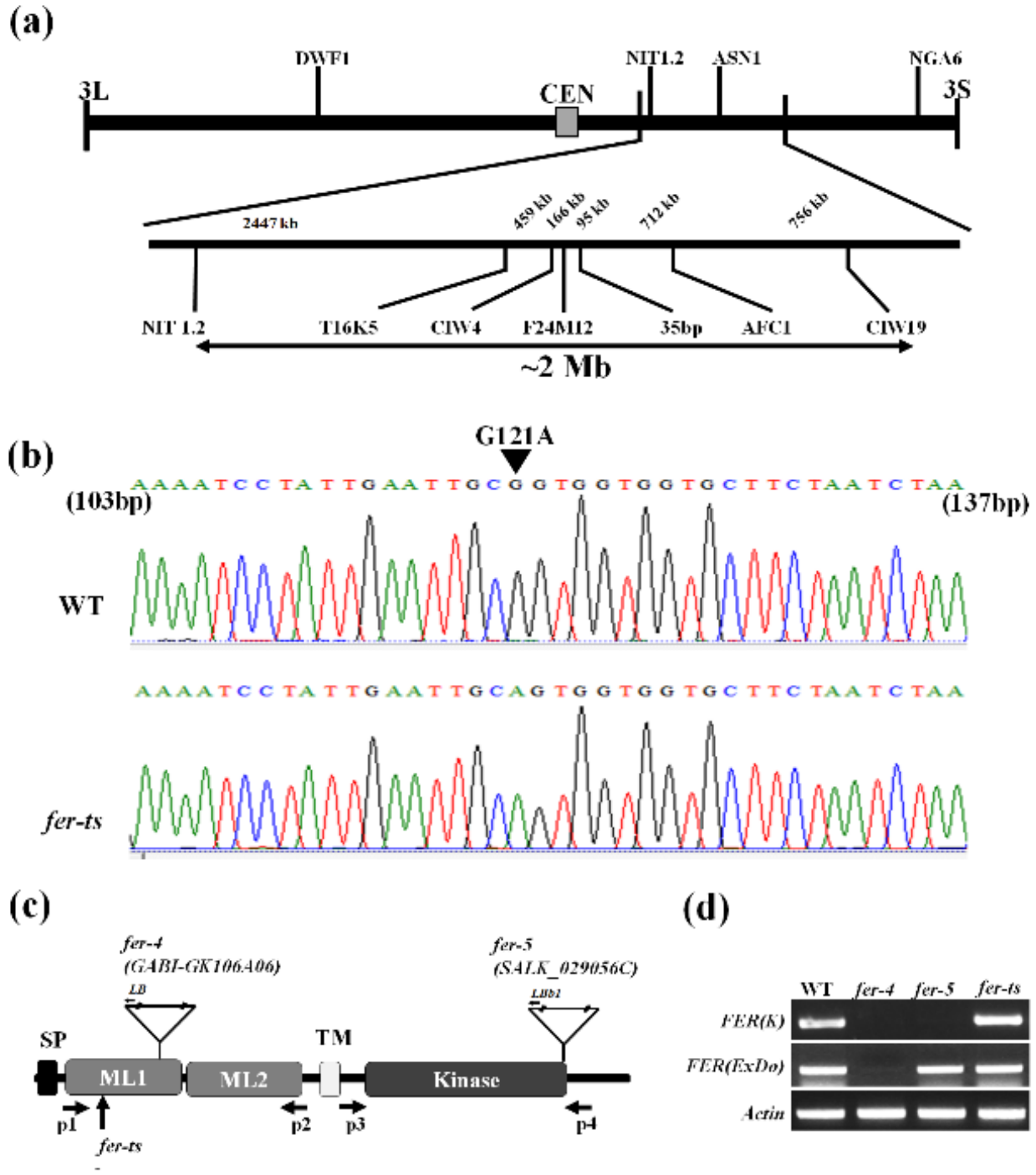

Figure 4. Map-based cloning of *fer-ts*.
(a) A linear diagram of the Arabidopsis third chromosome is shown, with a magnified F24M12 marker region displayed below. The centromere is indicated with filled-rectangle. Low-resolution map-based cloning resulted in identification of the *fer-ts* locus within an approximately 2 Mb region of chromosome III bounded by markers NIT1.2 and CIW19 (Double headed arrow). (b) SNPs specific to the ts-mutant within this region were identified using whole genomic resequencing, followed by targeted resequencing of genomic DNA sequencing of *fer-ts* and wild-type parental lines. A single G→A substitution was found in *FERONIA* (At3g51550). The arrowhead indicates G121A substituted mutation in *FERONIA* gene locus. (c) Schematic diagram of FERONIA protein domains and mutation regions, composed of an N-terminal extracellular domain (tandem repeat malectin-like domains; ML1 and ML2), TM (transmembrane) domain in the middle region and a C-terminal kinase domain (serine/threonine kinase), end of N-terminus has signal peptide (SP) sequence for plasma-membrane trafficking. The *fer-4* and *fer-5* mutants displayed that T-DNA was inserted in malectin-like domain 1 and kinase domain, respectively. (d) RT-PCR analysis of T-DNA inserted mutants and EMS mutants. The FER(K) and FER(ExDo) domains were amplified using P1 and P2 primers and P3 and P4 primers, respectively. Actin was used as a loading control.

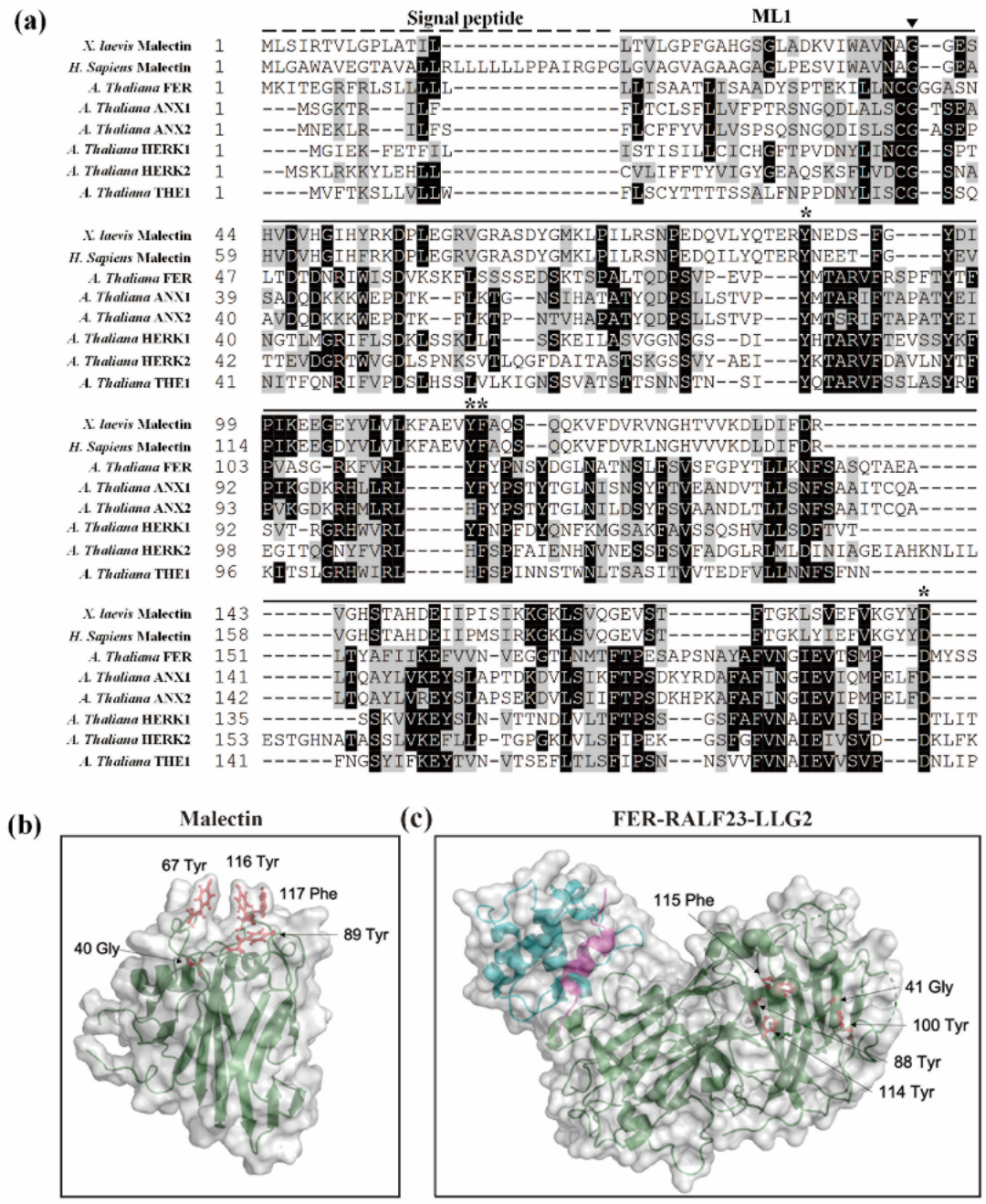

Figure 5. Localization of the highly conserved glycine mutation in fer-ts in *A. thaliana* FERONIA:RALF23:LLG2 and *X. laevis* malectin structures. (a) Several residues important for binding carbohydrate ligands are conserved in plant CrRLK1L receptor kinase family members. Sequences analyzed include animal Malectin (*X. laevis* and *H. sapiens*) FERONIA and other well-characterized CrRLK1L homologs in *A. thaliana* (ANXUR1; ANX1, ANXUR1; ANX2, HERCULES1; HERK1 and THESEUS1; THE1). Putative N-terminal signal peptides are indicated as black dashed lines, and malectin and CrRLK1L ML1 domains by solid lines, respectively. The highly conserved G41 of FER is marked by arrowhead. Black boxes indicate fully conserved residues; shaded boxes indicate similar and partially conserved residues. Conserved residues that have been shown to participate in binding nigerose in the *X.laevis* malectin structure are marked by asterisks. Sequence alignment analysis was performed by CLUSTAL Omega program (http://www.ebi.ac.uk/Tools/msa/clustalo/) and displayed by using BOXSHADE software (www.ch.embnet.org/software/BOX_form.html). (b) Crystal structure of the *X. laevis* malectin protein (PDB ID: 2K46) with binding pocket aromatic residues and the highly conserved glycine residue based on sequence similarity to FER shown in red. (c) Crystal structure of FER protein (green) in complex with RALF23 ligand (magenta) and GPI-anchored protein LLG2 (blue) (PDB ID: 6A5E). No analogous binding pocket is observed on the ML1 domain, as all conserved aromatic residues (red) are buried within the protein. Both (b and c) were generated using PyMol (DeLano Scientific).

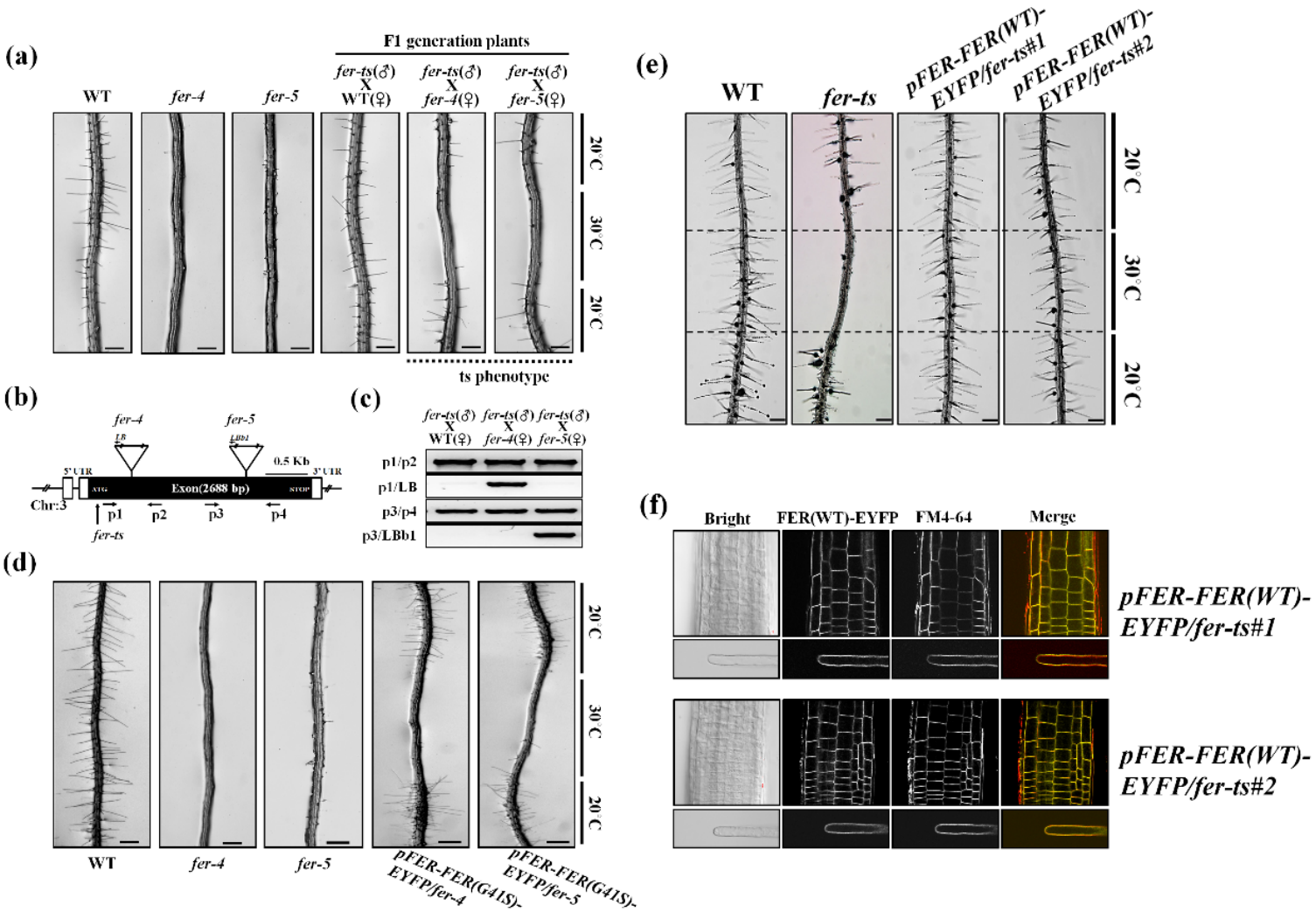

Figure 6. The *fer-ts* mutant confers ts-root hair growth defects when crossed with *fer-4* and *fer-5* mutants. (a) Wild-type (WT), *fer-4, fer-5*, and F1 progeny from crosses (paternal = *fer-ts*, maternal = *fer-4* or *fer-5*) of *fer-ts/fer-4* and *fer-ts/fer-5* were grown vertically for seven days at 20ºC, transferred to 30ºC for 6 h, and then grown for an additional 24 h at 20ºC. Both *fer-ts/fer-4* and *fer-ts/fer-5* progeny clearly demonstrated a ts-dependent root hair phenotype. Scale bars = 200 µm. (b) Schematic diagram of the *FERONIA* gene structure. Open and filled boxes indicate untranslated regions (UTRs) and exon regions, respectively. The locations of T-DNA insertion mutants (*fer-4* and *fer-5*) and *fer-ts* are indicated by triangles and arrows, respectively. (c) Genotyping of crossed F1 plants. Genomic DNA was extracted from F1 generation plants and subjected PCR to confirm presence of the *fer-4* and *fer-5* genotypes (d) Both *fer-4* and *fer-5* display temperature-dependent root hair phenotypes when transformed with a fluorescently-tagged FER construct containing the *fer-ts* mutation (pFER-FER(G41S)-EYFP). Seven-day old seedlings stably transformed and homozygous for (pFER-EYFP(G41S)-EYFP) were grown vertically at 20ºC, transferred to 30ºC for 6 h, and then grown for an additional 24 h at 20ºC. Presence of the transgenic pFER-FER(G41S)-EYFP construct clearly demonstrated a ts-dependent root hair phenotype. Scale bars = 200 µm. (e) Temperature sensitive root hair growth defects of *fer-ts* are fully rescued when transformed with a fluorescently-tagged FER construct (pFER-FER(WT)-EYFP). Seven-day old seedlings stably transformed and homozygous for (pFER-EYFP(WT)-EYFP)were grown vertically at 20ºC, transferred to 30ºC for 6 h, and then grown for an additional 24 h at 20ºC. Bright field images were collected with a Nikon Eclipse E600 wide-field microscope with a 10x Plan Apo DIC (0.75 NA) lens. (f) Subcellular localization of FER(WT)-EYFP protein in roots and root hairs in a rescued *fer-ts* mutant plant. Fluorescent confocal images displaying the subcellular distribution of FER(WT)-EYFP protein was detected from growing root, and mature root hair cells of seven-day-old *fer-ts* seedlings stably transformed and homozygous for pFER-FER(WT)-EYFP. Cells were counter-stained by incubating for 5 min in a FM4-64 to visualize cell membranes. Images were collected by spinning-disk fluorescence confocal microscopy using a Zeiss 40x Plan-Apochromat (1.3 NA) lens with appropriate EYFP and FM4-64 fluorescence filter sets. Scale bars = 20 µm.

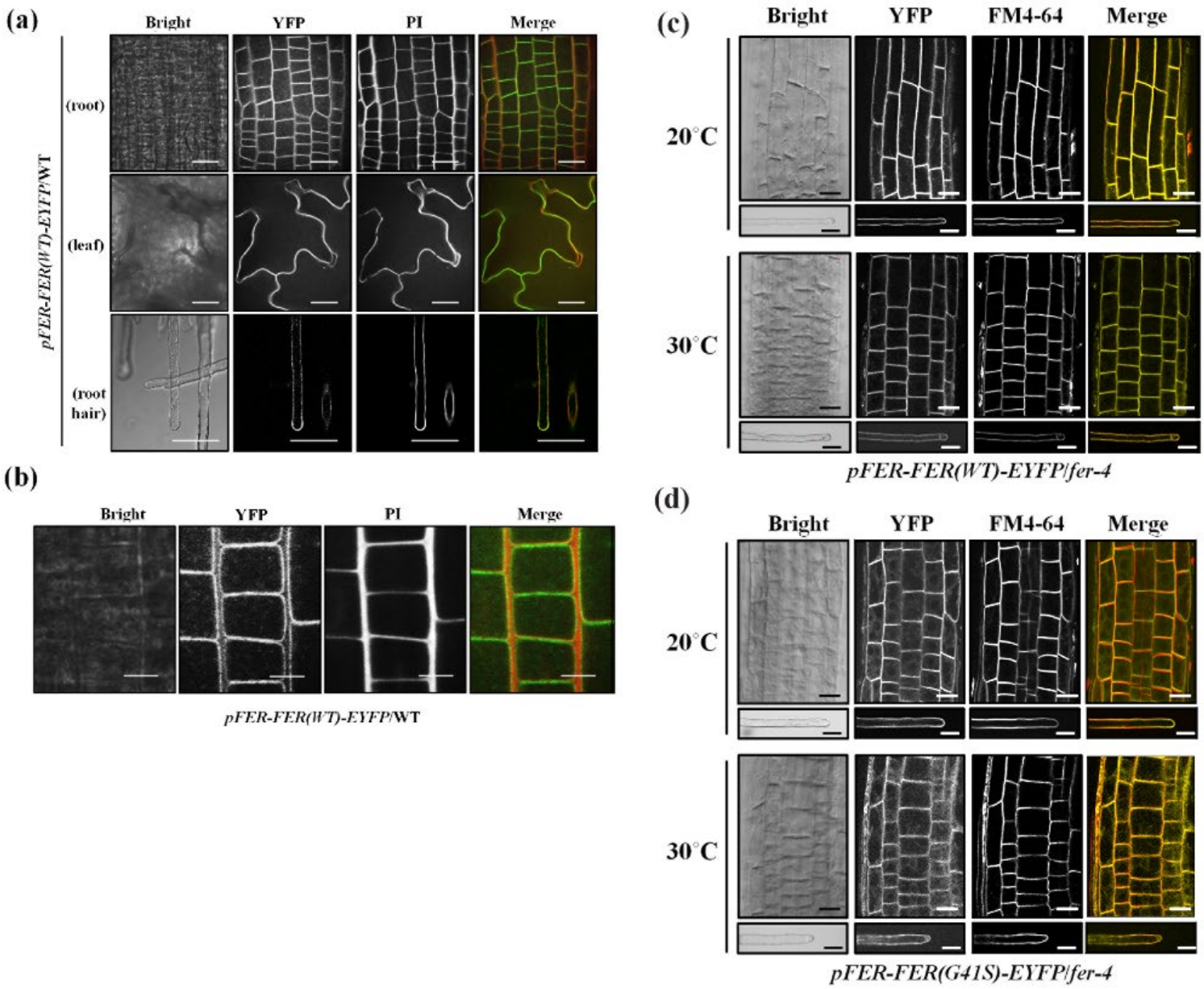

Figure 7. Subcellular localization of FER(WT)-EYFP and FER(G41S)-EYFP fluorescent fusion proteins in stably transformed *Arabidopsis*. (a) Subcellular localization of FER(WT)-EYFP protein in various tissues. Fluorescent confocal images displaying the subcellular distribution of FER(WT)-EYFP protein was detected from growing root, leaf and root hair cells of seven-day-old seedlings in *pFER-FER(WT)-EYFP*/WT transgenic plants. Cell walls were counter-stained by incubating for 5 min in a propidium iodide (PI) solution (10 µg/ml). Images were collected by spinning-disk fluorescence confocal microscopy using a Zeiss 40x Plan-Apochromat (1.3 NA) lens with appropriate EYFP and PI fluorescence filter sets. Scale bars = 20 µm. (b) Magnified images of FER(WT)-EYFP fluorescence. FER(WT)-EYFP in wild-type of growing root cells of seven-day-old *A. thaliana* seedlings was detected by spinning-disc confocal microscopy using a Zeiss 100x Plan-Apochromat (1.46 NA) oil immersion objective with appropriate EYFP and PI filter sets. Scale bars = 10 µm. (c-d) Subcellular localization of FER(WT)-EYFP (c) and FER(G41S)-EYFP (d) fluorescent fusions in root and root hair cells at normal (20ºC) and elevated (30ºC) temperatures. Cells from *fer-4* plants stably transformed and homozygous for FER(WT)-EYFP or FER(G41S)-EYFP were counterstained with FM4-64 (5 µM) for five minutes to visualize cell membranes. Images were collected by spinning-disk fluorescence confocal microscopy using a Zeiss 40x Plan-Apochromat (1.3 NA) lens with appropriate EYFP and FM4-64 fluorescence filter sets. Scale bars = 20 µm; root, 10 µm; root hair.

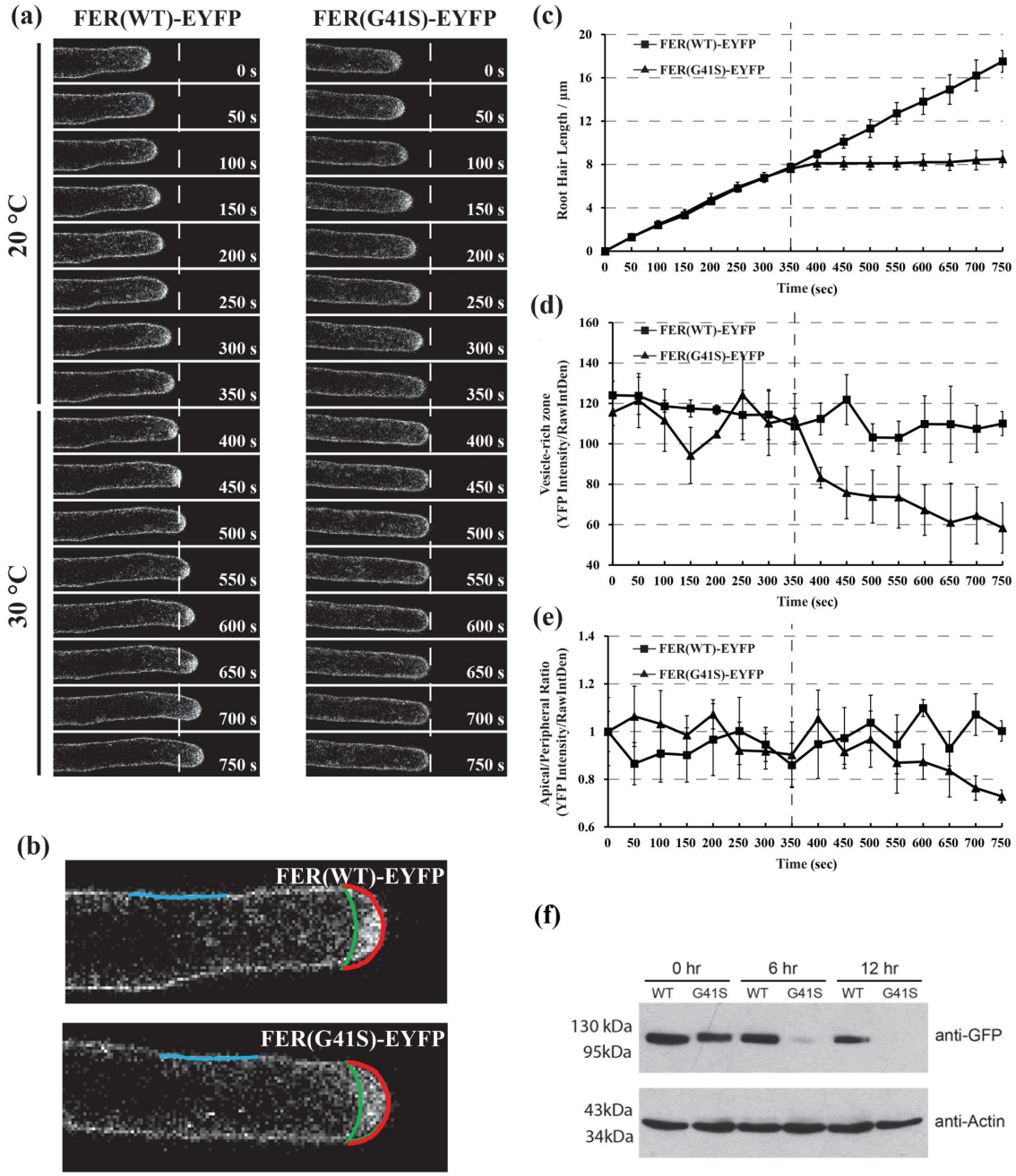

Figure 8. Subcellular localization dynamics of FER(WT)-EYFP and FER(G41S)-EYFP proteins in growing root hair cells under both normal (20ºC) and elevated (30ºC) temperatures. (a) Root hair tip-growth in stably transformed lines expressing FER(WT)-EYFP and FER(G41S)-EYFP fluorescent fusion proteins under (20°C) and (30°C) temperature by time-lapse microscopy. Confocal images of were acquired using a Leica confocal laser-scanning microscope SP8 with a 63x oil lens (Numerical Aperture = 1.4) with 5s intervals. Representative images are presented at 50s intervals (10 frames). Scale bar: 10 µm. (b) Schematic diagram shown areas and lines used for fluorescence intensity quantification. Apical (red line) and peripheral (blue line) plasma membrane domains were measured, and the area between the apical plasma membrane and green line represents the vesicle-rich zone. (c) Quantitative analysis of root hair growth in stably transformed lines expressing FER(WT)-EYFP (n=3) and FER(G41S)-EYFP (n=3). Root hair elongation was measured every 50s using the measurement function in ImageJ. (d) Quantitative analysis of YFP intensity of vesicle-rich zone. (e) Quantitative analysis of YFP intensity of apical/ peripheral ratio. Values are normalized using 0s as 100%. The dashed line indicates time point of transition from permissive (20°C) to (30°C). Error bars in (c, d, e) represent SD. (f) Protein turnover rates of FER(WT)-EYFP and FER(G41S)-EYFP at elevated temperature (30ºC). Five-day old seedling were grown at 20ºC and then treated with 200 µM cycloheximide and transferred to 30ºC. Total proteins were extracted at each time point and the relative levels were determined using immunoblotting with anti-GFP and anti-actin antibodies. FER(G41S)-EYFP levels rapidly decreased during the time course, while levels of FER(WT)-EYFP were not significantly reduced. Actin was used as a loading control.

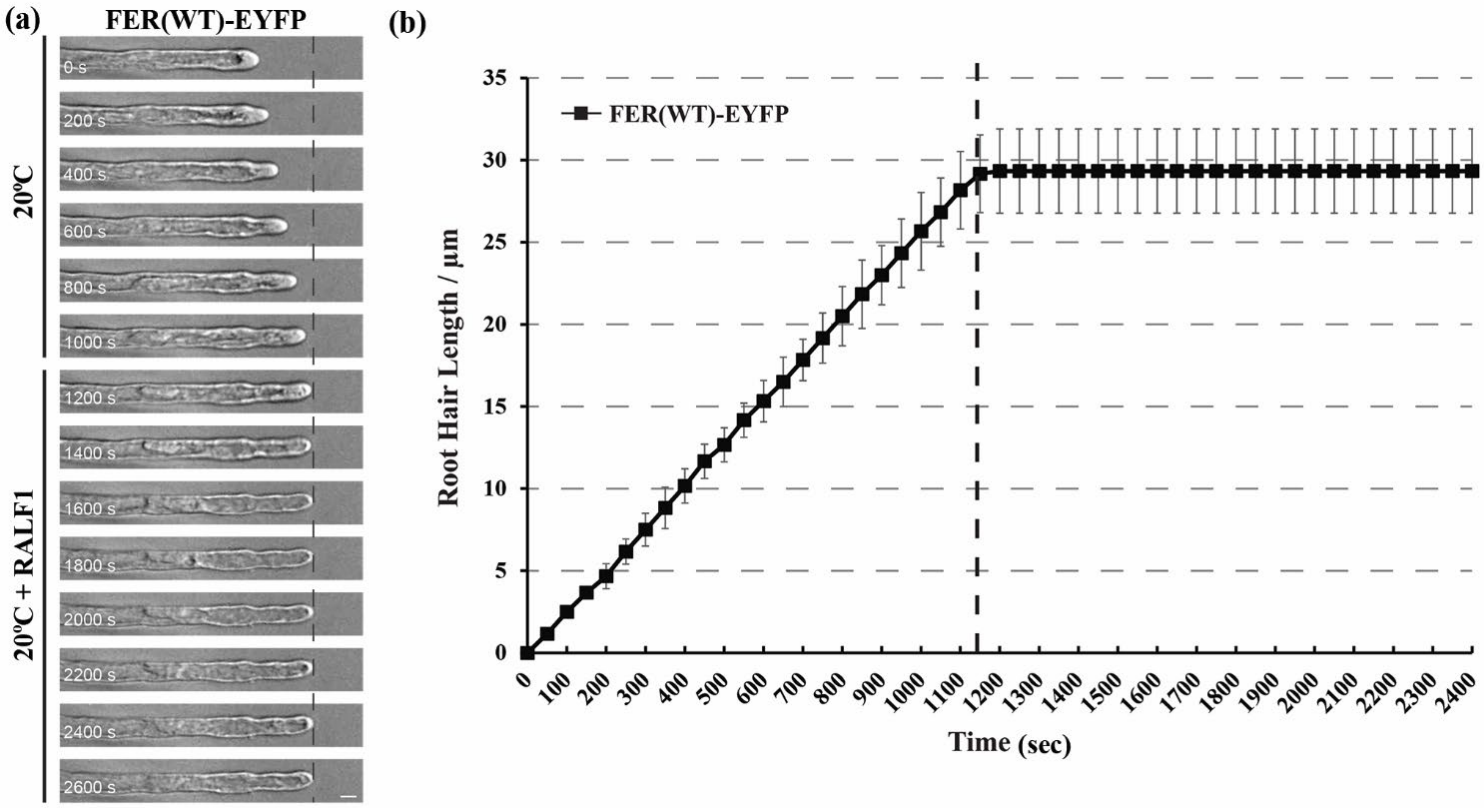

Figure 9. RALF peptide treatment terminates root hair growth in FER(WT)-EYFP expressing line.
(a) Root hair tip-growth in stably transformed lines expressing FER(WT)-EYFP fluorescent fusion protein under permissive (20°C) temperature by time-lapse microscopy. Bright field images of growing root hair cells (n=3) were collected using a Nikon Eclipse E600 wide-field microscope with a 10x Plan Apo (0.45 NA) lens with 5s intervals. The dashed line represents when media containing RALF1 (1 µM) was perfused into the growth chamber. Representative images are presented at 200s intervals. Scale bar: 50 µm. (b) Quantification of root hair growth. Root hair elongation was measured every 50s using the measurement function in ImageJ. Error bars represent SD.

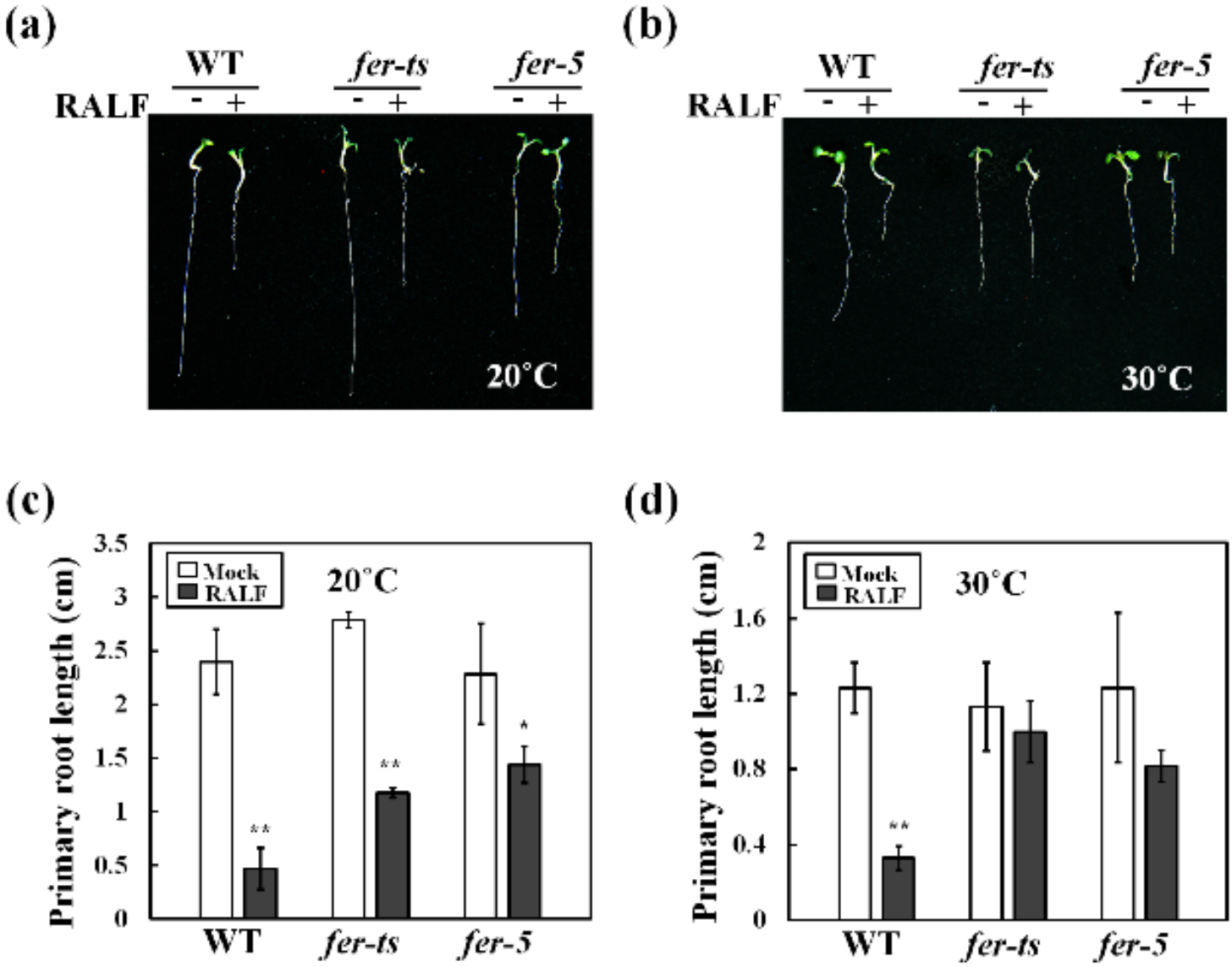

Figure 10. *fer-ts* mutants are partially insensitive to RALF1 peptide mediated root growth inhibition at elevated temperatures. Wild-type (WT), *fer-ts*, or *fer-5* plants were germinated and grown for 3 days in ½ MS liquid media at 20ºC, and then transferred to ½ MS liquid media containing 1uM RALF1 peptide (RALF+) or a mock buffer control (RALF-) and grown an additional 3 days at 20ºC (a) or 30ºC (b). Images of representative seedlings were collected using an Olympus SZX12 stereoscopic microscope. Quantification of primary root lengths (n = 10 seedlings) in the presence or absence of RALF1 peptide treatment in normal, 20˚C (c) and elevated, 30ºC (d) conditions. Primary root lengths were determined using Image J. Error bars represent SD. *p<0.05, **p<0.01 by Student's *t*-test.

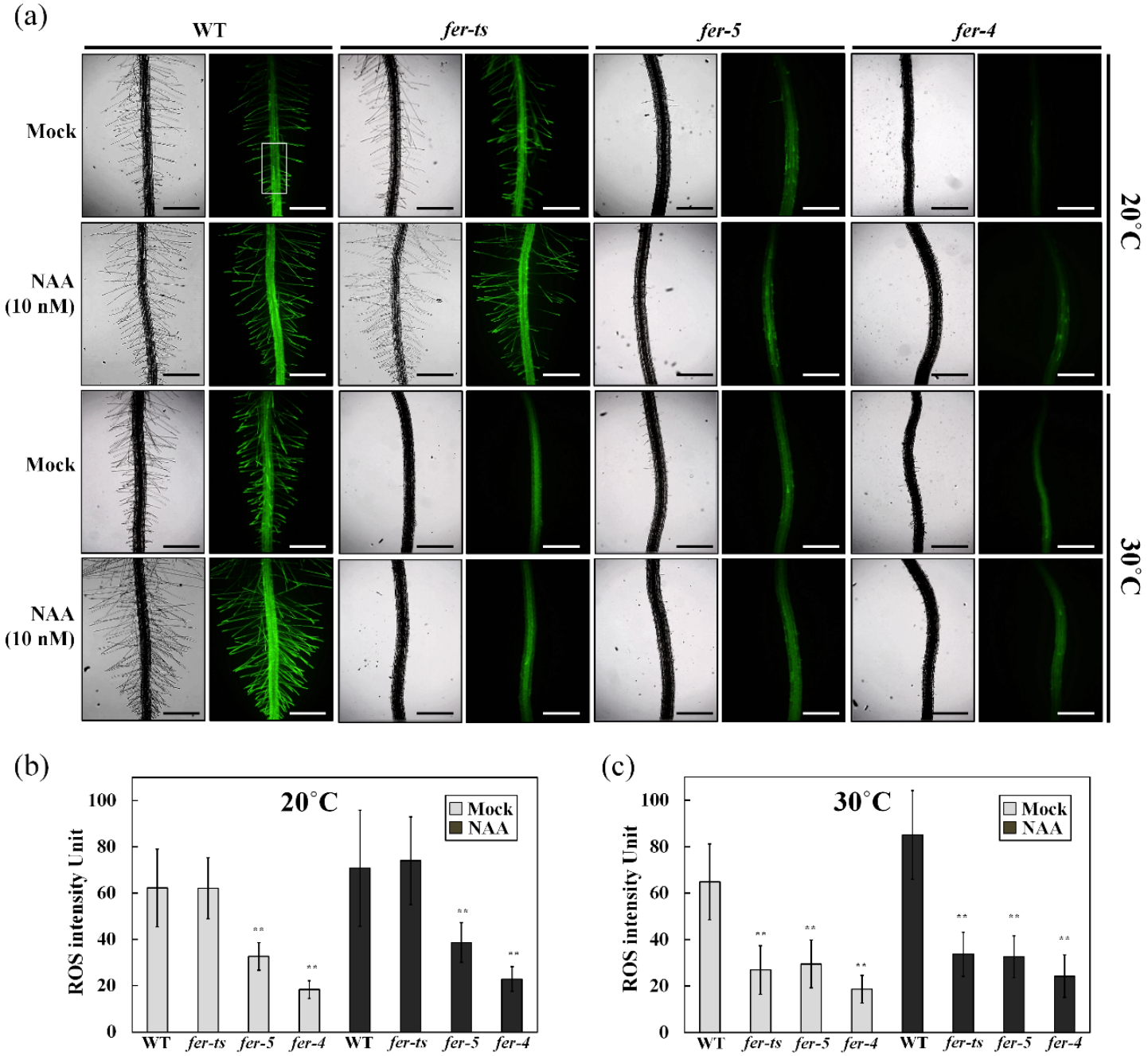

Figure 11. Detection of ROS in WT, *fer-ts* and *fer-5* primary roots and root hairs.
(a) ROS accumulation in normal and elevated temperature conditions with or without auxin treatments. Wild-type (WT), *fer-ts*, *fer-4*, or *fer-5* seedlings were grown vertically on ¼ MS media plates for seven days at normal (20ºC) or elevated (30ºC) temperatures in the presence or absence of (10 nM NAA). Plates were bathed with five ml of 50 uM in H_2DCF-DA suspended in ¼ MS liquid media for 5 min, followed by two gentle washes with 10 ml of ¼ MS. Fluorescence images were collected with a Zeiss Axio Imager Z1 fluorescence microscope with 2.5x objective and green (GFP) filter set. The WT ROS image was acquired by auto-exposure, all other images were acquired using the WT exposure conditions. Scale bars = 500 µm. (b) The rectangle in (a) indicates a representative region of interest (ROI) where average ROS intensity was quantified for the samples. Intensities of ROS were quantified by image J program. Error bars represent SD. **$p<0.01$ by Student's *t*-test.

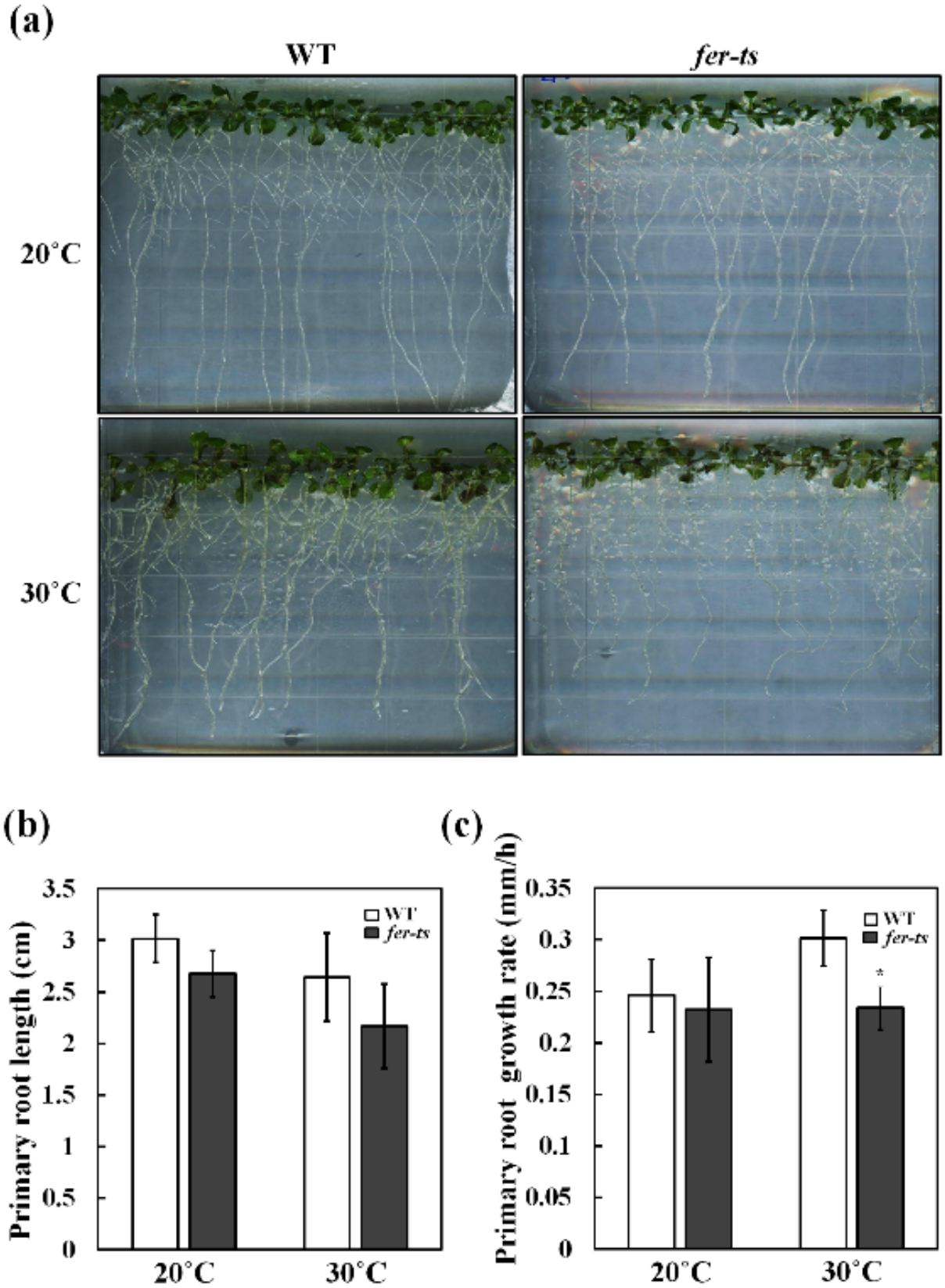

Figure S1. Primary root growth of *fer-ts* mutants under normal and elevated temperature conditions. (a) Photographs of wild-type and *ltl2* mutant under permissive and non-permissive temperature conditions. (b) Measurements of primary root growth length under normal (20ºC) and elevated (30ºC) temperature conditions. (c) Primary root growth rate under 20˚C and 30˚C conditions. (a)-(c) Seven day-old wild-type (WT; n=25) and *fer-ts* (n=25) seedlings were transferred to the 30˚C for two weeks and primary roots were scanned by EPSON 4990 photo scanner every second day. The primary roots length were determined using Image J, and root growth rates were calculated by dividing growth by 48 hours (mm/h). Error bars represent SD. *$p<0.05$ by Student's *t*-test.

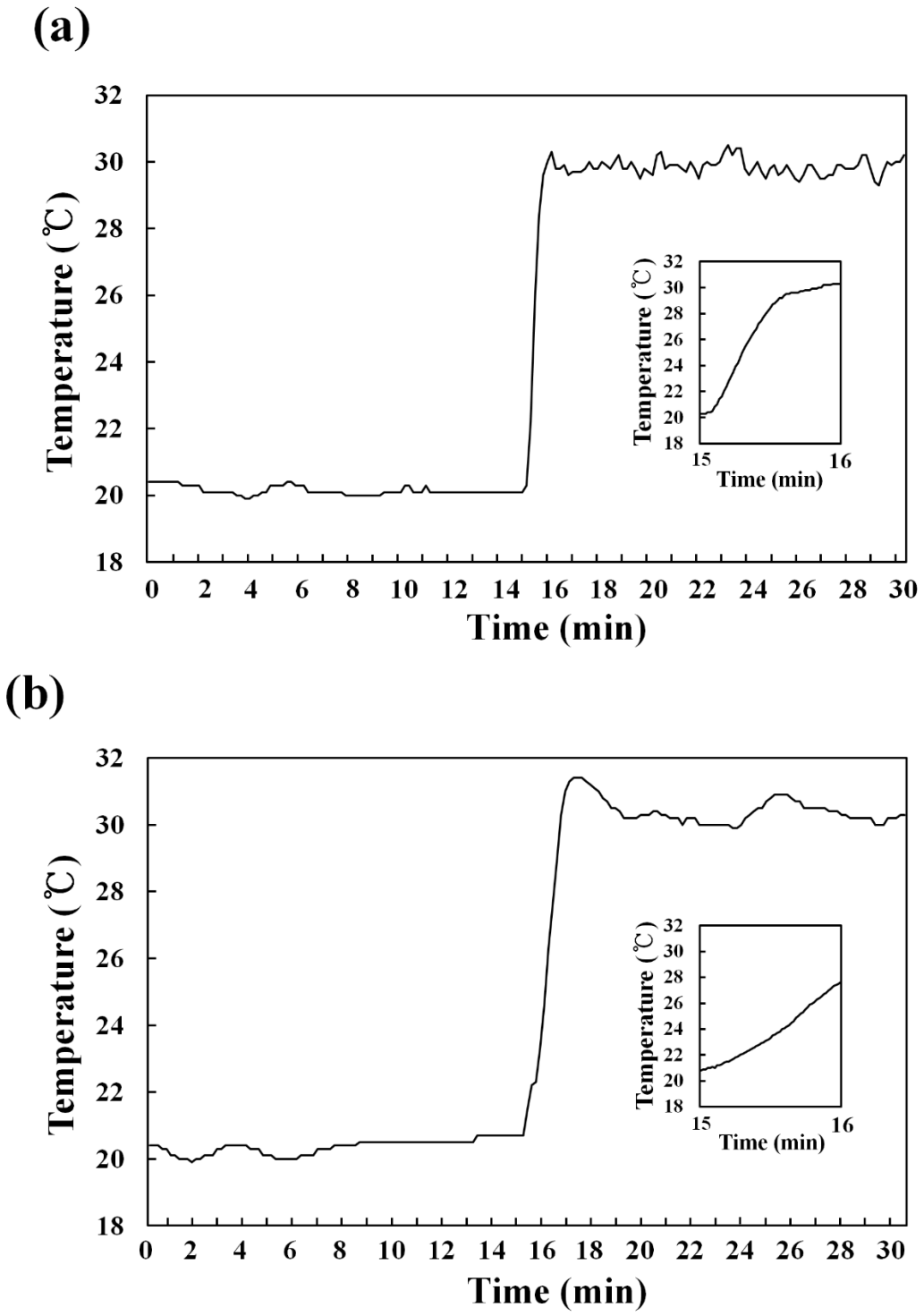

Figure S2. Root hair growth chamber temperature measurement during transition from normal (20ºC) to elevated (30ºC) temperature conditions.

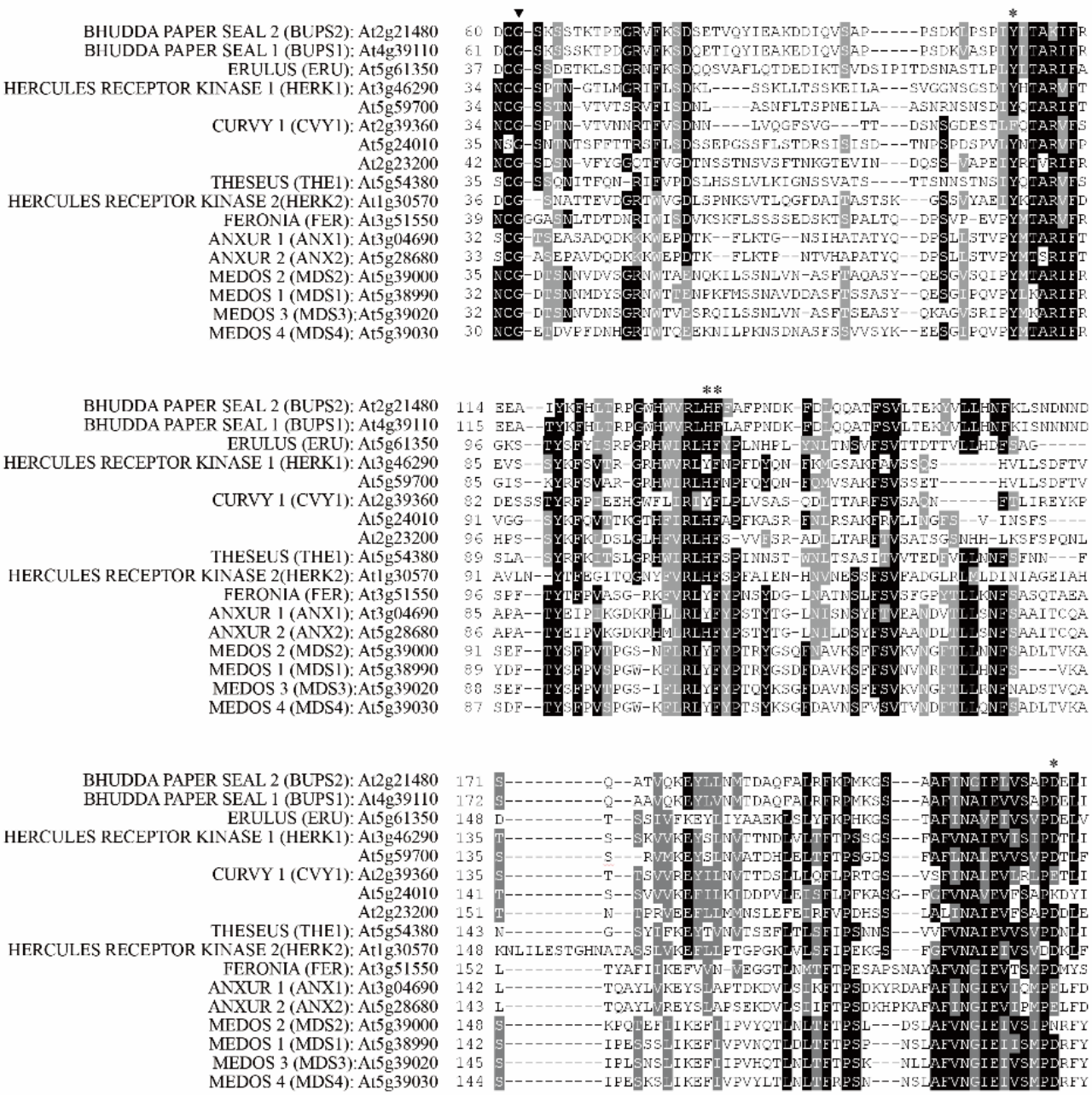

Figure S3. Sequence alignment of *Arabidopsis* CrRLK1L subfamily receptor kinases.
Multiple-sequence alignment analysis was performed with the Clustal Omega program (http://www.ebi.ac.uk/Tools/msa/clustalo/) and displayed using BOXSHADE (www.ch.embnet.org/software/BOX_form.html). Sequence similarity analysis of CrRLK subfamily members in Arabidopsis. *At3g51550* encodes FERONIA protein. The highly conserved FERONIA G41 and additional putative key residues are marked by black arrowheads and asterisks, respectively. Black boxes indicate conserved residues; shaded boxes indicate residues with conserved substitutions.

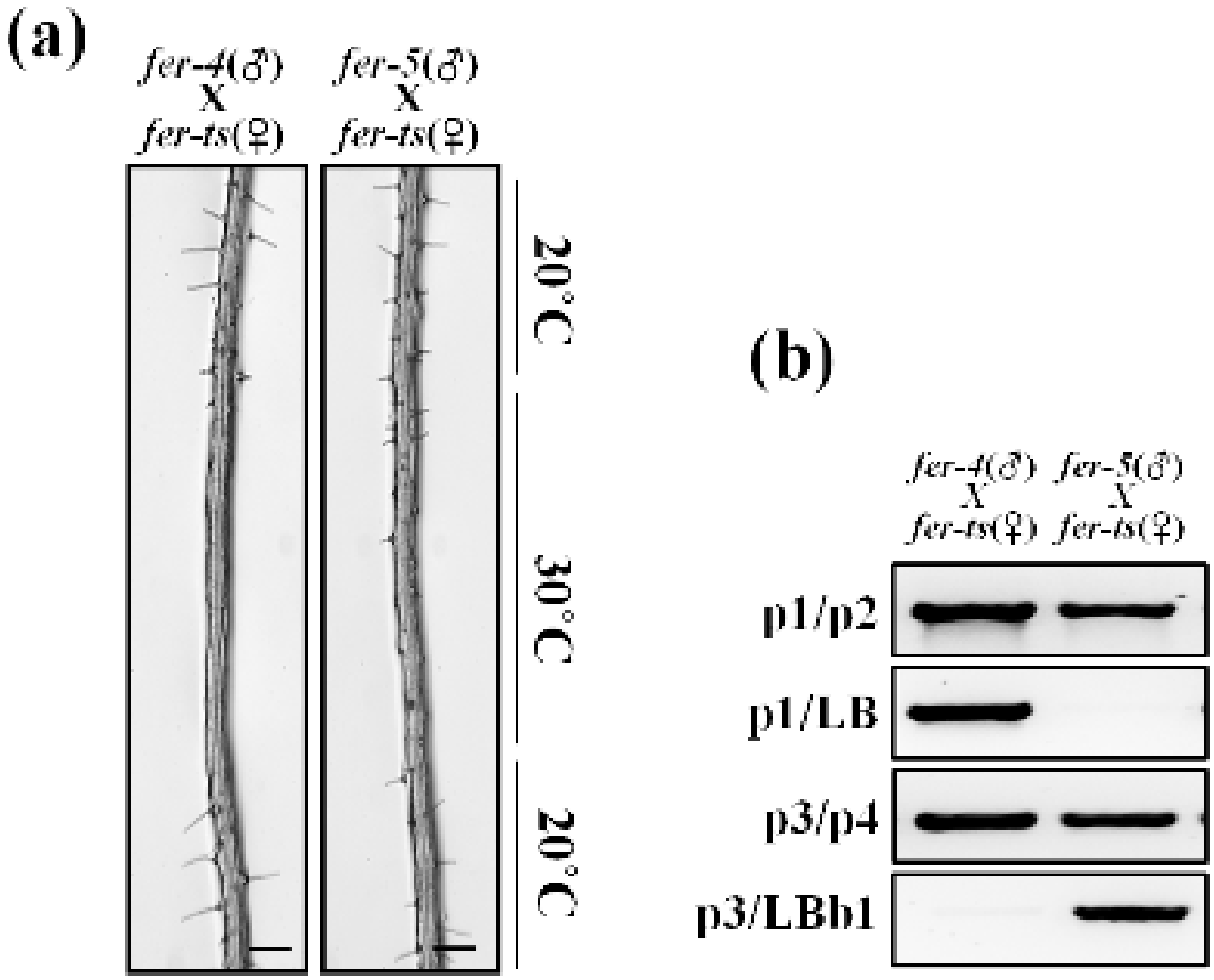

Figure S4. Temperature-sensitive root hair growth in *fer-ts/fer-4* and *fer-ts/fer-5* F1 plants.
(a) Wild-type (WT), *fer-4, fer-5*, and F1 progeny from crosses (maternal = *fer-ts*, paternal = *fer-4* or *fer-5*) of *fer-ts/fer-4* and *fer-ts/fer-5* were grown vertically for seven days at 20ºC, transferred to 30ºC for 6 h, and then grown for an additional 24 h at 20ºC. Both *fer-ts/fer-4* and *fer-ts/fer-5* progeny clearly demonstrated a ts-dependent root hair phenotype. Scale bars = 200 µm. (b) Genotyping of crossed F1 plants. Genomic DNA was extracted from F1 generation plants and subjected PCR to confirm presence of the *fer-4* and *fer-5* genotypes.

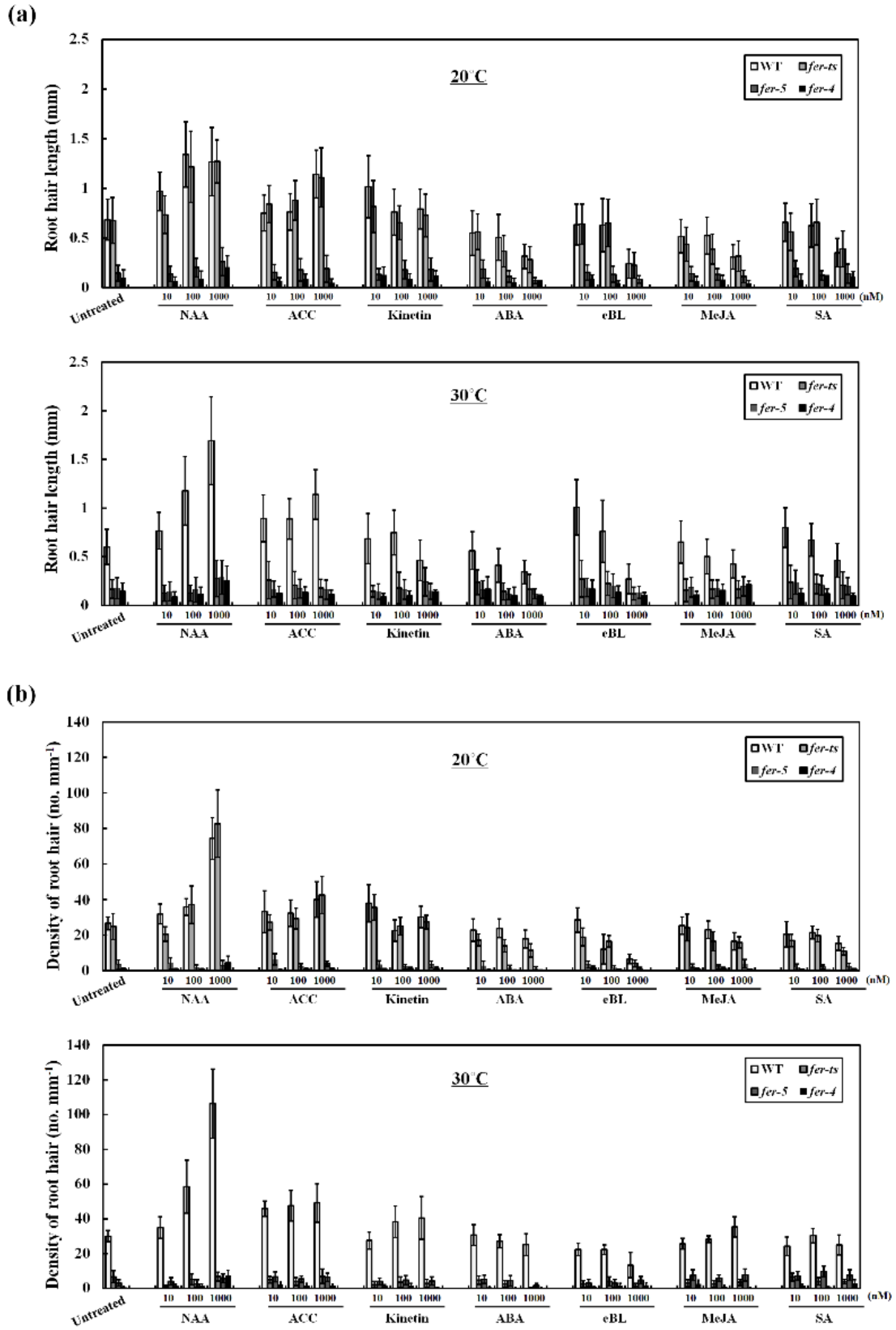

Figure S5. In elevated temperatures, *fer-ts* responds to hormone treatments similarly to *fer-4* and *fer-5* mutants. (a and b) Quantification of root hair length and density in normal (upper panels) and elevated temperature (lower panels) in 10, 100, and 1000 uM concentrations for each of the various hormone treatments (NAA; Auxin, ACC; ethylene, Kinetin; Cytokinin, ABA; Abscisic acid, eBL; epi-brassinosteroid, MeJA; methyl jasmonic acid, SA; Salicylic acid). Three-day-old seedlings were transferred into ½ MS liquid media containing three different concentrations of the various hormones. Then, transferred plants were incubated at 20˚C and 30˚C for seven days before quantification. The root hairs were photographed by Olympus AX-70 microscope and root hair length and densities were determined by image J. Error bars represent SD.

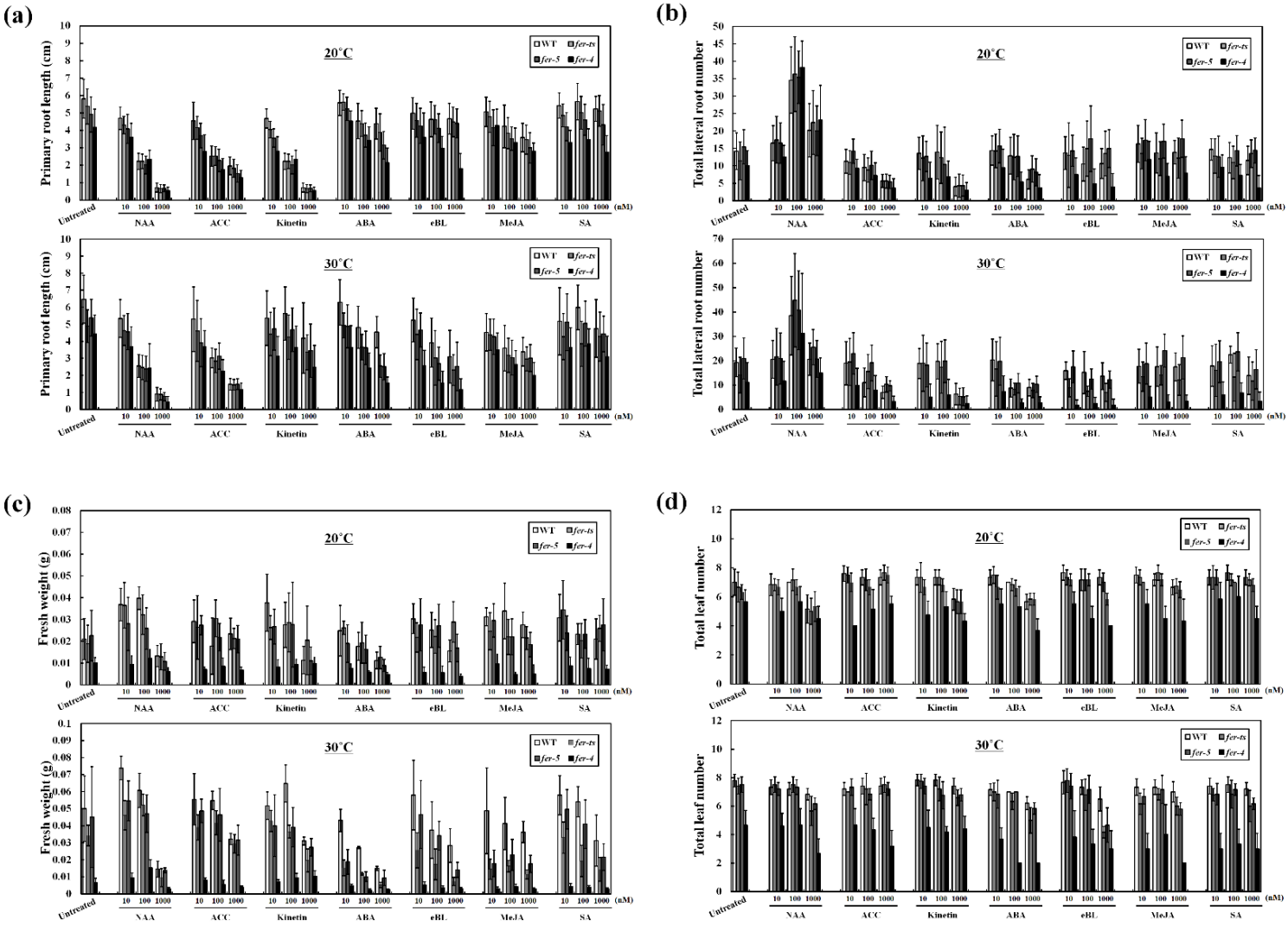

Figure S6. Hormonal effects on primary root length, total lateral root number, fresh weight and total leaf number in normal and elevated temperature conditions for *fer-ts*, *fer-4*, and *fer-5* plants. Primary root length (a), lateral root number (b), fresh weight (c), and leaf number (d) were measured in normal (upper panels) and elevated (lower panels) temperatures in 10, 100, and 1000 uM concentrations for each of the various hormone treatments (NAA; Auxin, ACC; ethylene, Kinetin; Cytokinin, ABA; Abscisic acid, eBL; epi-brassinosteroid, MeJA; methyl jasmonic acid, SA; Salicylic acid). Three-day-old seedlings (n=20 each for wild-type, *fer-ts*, *fer-4*, and *fer-5*) were transferred into ½ MS liquid media containing three different concentrations of the various hormones. Then, transferred plants were incubated at 20˚C and 30˚C for seven days before quantification. Error bars represent SD.